8-26-2015 12:00 AM

Dielectric Spectroscopy of Polyvinyl Alcohol Hydrogels and Nanocomposites

Nuwansiri N.K. Getangama
The University of Western Ontario

Supervisor
Dr. John R. de Bruyn
The University of Western Ontario Joint Supervisor
Dr. Jeffrey L. Hutter
The University of Western Ontario

Graduate Program in Physics

A thesis submitted in partial fulfillment of the requirements for the degree in Master of Science

DIELECTRIC SPECTROSCOPY OF POLYVINYL ALCOHOL HYDROGELS AND NANOCOMPOSITES

(Thesis format: Monograph)

by

Nuwansiri Getangama

Graduate Program in Physics

A thesis submitted in partial fulfillment

of the requirements for the degree of

Master of Science

The School of Graduate and Postdoctoral Studies

The University of Western Ontario

London, Ontario, Canada

Abstract

Gels based on polyvinyl alcohol (PVA) can be formed by repeated freezing and thawing of a solution of the polymer. PVA cryogels have applications as biomaterials, including artificial tissue and drug delivery systems. The mechanical and electrical properties of polymeric materials can be changed significantly by adding a small amount of nanometer-sized particles. In this work, the dielectric properties of PVA solutions and gels were studied in the frequency range from 10 μHz to 1 MHz as a function of temperature, using a dielectric spectrometer.

Comparison of the dielectric constant of a PVA solution to that of water indicates that –OH groups on the polymer make a large contribution to the dielectric response. The real and imaginary parts of the permittivity $\varepsilon(\omega)$ decrease during the cooling phase of a freeze-thaw cycle due to a reduction in the mobility of the dipoles, and do not completely recover upon thawing. Measurements of the loss tangent indicates the presence of three major relaxation processes in the PVA cryogel. One of them was similar to the process observed in water dielectric. The other two relaxation processes are identified as with α and β relaxation of the PVA molecules. Similar to water, all the relaxation peaks in the loss tangent move to lower frequency as the temperature is decreased due to a slowing of the relaxation processes. We observed a critical temperature at which the permittivity drops suddenly during the cooling portion of the freeze-thaw cycles. We identify this with the formation of micro crystals of PVA in the cryogel. Adding carbon nanotubes to the PVA solution raises this critical temperature. We interpret these results in terms of the structural changes that take place within the PVA gel in the process of gel formation. Overall, we have shown that dielectric spectroscopy data can be used to obtain useful information about PVA cryogels and nanocomposites.

Keywords: Polyvinyl alcohol (PVA), Dielectric spectroscopy, Carbon nanotubes, Polymer nanocomposites

Acknowledgements

I would like to express my deepest gratitude to my supervisors Dr. John de Bruyn and Dr. Jeffrey Hutter for their supervision and guidance throughout my work. Their patience and persistent motivation helped me to continue the research and writing the thesis.

I would also like to thank my advisory committee members Dr. Lyudmila Goncharova and Dr. Mahi Singh for insightful comments and interesting discussions which increased my understanding and interest in my field.

I am thankful to Dr. Mark Workentin and his research group members Pierangelo Gobbo, Wilson Luo, Praveen Gunawardene, Vaishnavi Somasundaram, Kathleen Winger, Tommaso Romagnoli and Sara Ghiassian for their guidance in the process of purification of carbon nanotubes.

My special thanks go to my colleagues Cameron Hopkins, Yang Liu, Maria Goiko, Maryam Mozaffari, Ruiping Ge and Colin Versnick in Dr. de Bruyn's research group and Himasha wijesekara, Jagan Sivakumaran in Dr. Hutter's research group for stimulating discussions and being a great team. I also thank fellow graduate students and all faculty and staff in my department for their friendly and kind support.

I also thank my parents, three sisters and their families for continuous support and encouragement throughout my life. I am specially thankful to my wife Jayanayana for her love, support and understanding.

Contents

List of Figures

List of Tables

Chapter 1

Introduction

1.1 Overview

In this Chapter, we introduce the main concepts underlying the work presented in his thesis. We then review the literature on polyvinyl alcohol (PVA), which is the polymer studied here, and discuss previous work on dielectric spectroscopy of polymers and nanocomposites. We then present the motivation for our work and discuss potential applications of PVA and its nanocomposites.

1.2 Polymers, nanocomposites and gelation

1.2.1 Polymers

Polymers are large molecules that can be described as a collection of repeated chemical units that are linked by covalent bonds. The repeated unit is called a monomer. A single polymer molecule can consist of thousands or more monomers. Polymers can be classified as homopolymers and heteropolymers. The former contain only one type of monomer, while the latter contains two or more different monomers. Polyethylene is an example of a homopolymer, while proteins are heteropolymers containing up to 20 different types of amino acid monomers.

Ideal, polyvinyl alcohol can be considered to be a homopolymer. However, commercial PVA contains some residual vinyl acetate groups as PVA is made by hydrolysis of polyvinyl acetate in methanol [1]. Therefore, commercial PVA is a copolymer of vinyl alcohol and vinyl acetate. We used 99% hydrolyzed PVA that contains 99% vinyl alcohol and 1% vinyl acetate.

1.2.2 Carbon nanotubes

Carbon nanotubes (CNTs) are made of single-atom-thick tubes of carbon. In graphene, which consists of planar sheets of carbon atoms, each carbon atom bonds with its three nearest neighbour carbon atoms, and each atom has an unbonded electron that is delocalized over the entire graphene layer. These delocalized electrons are able to carry electric current in graphene. A single-walled carbon nanotube (SWCNT) is a single graphene sheet rolled up to make a cylinder while multi-walled carbon nanotube (MWCNT) consist of multiple concentric graphene cylinders. Carbon nanotubes can be conductors or insulators, depending on their structure.

1.2.3 Nanocomposites

A polymer nanocomposite is a material made by adding nanometer-sized filler particles to a polymer to form a well-dispersed homogeneous blend. The filler particle size can be a few to tens of nanometers. The electrical and mechanical properties of nanocomposites can be very different from those of the pure polymer. This leads to the possibility of developing materials with particular desired properties. Researchers have used many different types of filler particles, such as calcium carbonate [2], glass beads or fibers [3], metal nanoparticles [4], and CNTs [5] to improve the properties of polymers. Some of the parameters that affect the properties of a composite are the size, volume fraction, shape and electrical conductivity of the filler particles. Introduction of a small amount of nanometer-sized particles such as carbon nanotubes can result in dramatic changes to the properties of polymers because of their high surface area to volume ratio, which leads to enhanced polymer filler-interactions.

1.2.4 Gelation

Polymer solutions can undergo a transition to a solid-like gel state either by chemical crosslinking or physical crosslinking. This transformation is known as gelation. In this work, we studied PVA solutions and dispersions of CNTs in PVA solutions. They both can undergo gelation by the formation of physical crosslinks (e.g., polymer-polymer entanglements, or the formation of crystallites that act as connections between chains) between PVA molecules [4]. As the number of physical crosslinks between PVA chains increases, the gels become stronger and more rigid.

1.3 Dielectric spectroscopy

The electromagnetic properties of materials have been studied in many ways. On the microscopic scale, the structure of the material, the energy bands of charge carriers, and magnetic moment of atoms and molecules are topics of substantial interest. The overall behaviour of a material under the influence of an external electric field provides more macroscopic information. Dielectric spectroscopy is one tool used to study macroscopic electrical properties of a material.

Dielectric spectroscopy involves measuring the dielectric properties of a material as a function of the angular frequency of an applied electric field. The primary dielectric property is the permittivity $\varepsilon(\omega)$ which characterizes the response of the material to an applied electric field. The main phenomena that contribute to permittivity are dipolar relaxation, atomic polarization, electronic polarization, and ionic relaxation. Each phenomenon dominates at a different frequency range, as shown in Fig. 1.1. Studying the permittivity spectrum of a material gives insights into the importance and time scale of each of these processes, and this information can be interpreted in terms of the structural properties of the material.

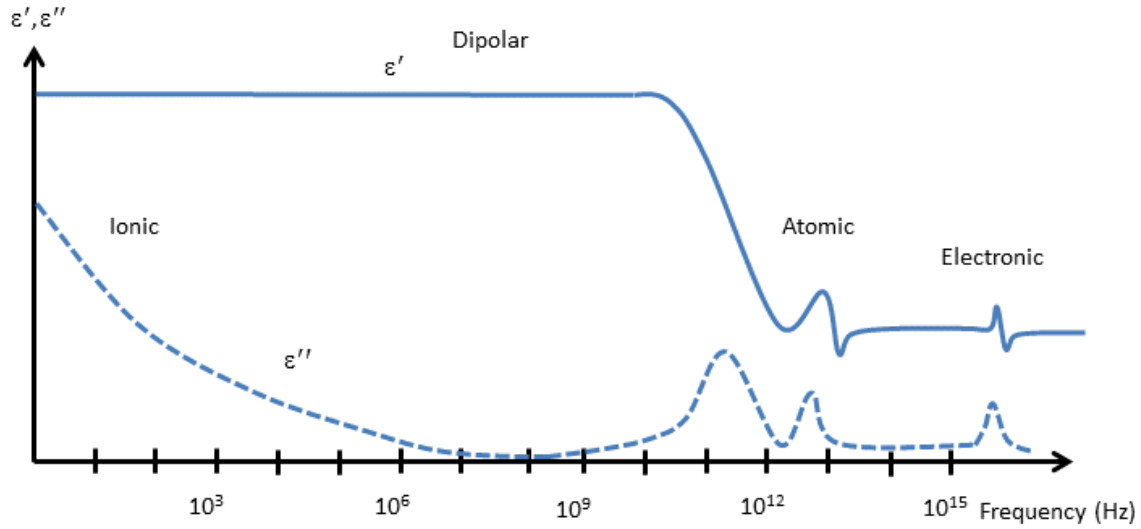

Figure 1.1: Schematic graph of the real ε' and imaginary ε'' parts of the complex permittivity $\varepsilon(\omega)$ as a function of frequency. The figure shows the contributions of different phenomena to the permittivity at different frequency ranges. For example, ionic conduction causes ε'' to increase at low frequencies.

Ionic conduction is the dominant contribution to ϵ'' at low frequencies. For example, free ions in a solvent move in response to an external electric field, producing an electric current. Atomic polarization results when adjacent positive and negative ions are exposed to an external electric field, causing their separation to change and inducing a dipole moment in the material. Electronic polarization is quite similar. The electron cloud of a neutral atom becomes distorted in an electric field, inducing a dipole moment in the atom. Dipolar polarization will be explained in Section 2.2.1 and is important in materials that contain molecules with permanent dipole moments, such as water. In our experiments, we see mainly effects due to ionic and dipolar relaxation as the frequency range we studied is between 10 mHz to 1 MHz.

1.4 Summary of previous work

1.4.1 Application of PVA hydrogels

Hydrogels are made from hydrophilic polymers and can absorb and store large amounts of water. A hydrogel has the ability to swell in water or biological fluids. A three-dimensional crosslinked hydrogel can be made by covalent bonds, hydrogen bonds or physical entanglements. The crosslinks prevent the hydrophilic polymer from dissolving in the liquid phase. Hydrogels are of great interest as biomaterials and for controlled drug delivery. Crosslinking agents used in chemical crosslinking can result in toxic residues. One of the main advantages of physical crosslinking in biomedical applications is that it avoids issues with toxicity. PVA gels have been of great interest for pharmaceutical and biomedical applications as they are non-toxic, bioadhesive, rubbery and elastic, and easy to make [6]. Researches have investigated the use of PVA gels for different possible applications, which are summarized here.

Becky et al. [7] produced PVA microparticles for controlled drug delivery using physical crosslinking made by repeated freezing and thawing as discussed in Section 3.4.2. They produced PVA microparticles with diameters from 150 to greater than 1400 μm. They attached bovine serum albumin proteins (BSA) to the PVA microgels and studied the release of BSA using UV absorbance. Koichi et al. [8] also studied PVA hydrogels made by freeze-thaw cycles. Their PVA hydrogel contained 80–90 wt% water. They implanted the gel into the dorsal muscles of rabbits for up to three months and observed neither degeneration nor death of muscle cells. Based on the properties of their gels, they suggested that PVA cryogels could be used for tissue replacement.

Millon et al. [9] explored the possibility of using PVA hydrogels as aortic replacements. They made PVA hydrogel tubes using the freeze-thaw method. After one freeze-thaw cycle, the diameter of the tube was increased by applying a strain. The tube was then treated with up

to six more freeze-thaw cycles. They found that the mechanical properties of the PVA tubes were similar to those of porcine aorta. The stress-strain behavior of their samples stayed the same over one year after preparation.

The dielectric properties of PVA hydrogels made by freezing and thawing were studied by Martha et al. [10]. They froze a 15 wt% PVA solution at –20 °C for 12 hours then heated the sample to 20 °C at a rate of 1.8 °C/min to complete one freeze-thaw cycle. Samples were subjected to a varying number of cycles, then dried in a vacuum oven at 25 °C until their weight was constant. They observed that the number of cycles affected the permittivity and that the dielectric loss tangent was lower than 1, meaning that dielectric behavior dominated over conduction.

PVA cryogels made by freeze-thaw cycles were studied as tissue-mimicking materials using magnetic resonance imaging (MRI) and ultrasound imaging [11]. These workers used 10% PVA solutions to construct cylindrical phantoms. The authors found that the speed of sound in their PVA phantoms was 1520–1540 m/s, which matched the typical range for tissue.

1.4.2 Previous work on polymer nanocomposites

Dielectric spectroscopy has been used previously to study the properties of polymer nanocomposites. Pötschke's group has studied nanocomposites made by melt mixing polycarbonate and multi-walled carbon nanotubes (MWCNT) having diameters of 10–15 nm and lengths of 1–10 μm [5]. They measured the complex permittivity and AC conductivity in the frequency range of 10^{-4} Hz to 10^{7} Hz. They found that the percolation threshold, which is the minimum MWCNT concentration needed to form a conductive network in the composite, was between 1.0 and 1.5 wt%. The unexpectedly high value of the threshold implied that only a fraction of the CNTs contributed to the conductive network in the composite as a result of aggregation of CNTs. As they varied the MWCNT concentration from 0 to 5 wt%, the conductivity changed

from on the order of 10^{-14} to 1 S/m. They studied the effect of sample preparation on dielectric properties by changing mixing parameters such as time and mixing speed.

1.5 Motivation and scope

Polymers have been used for many applications in everyday life such as electrical insulators, packing materials, and construction materials. In particular, polyvinyl alcohol has been of great interest as its relatively simple structure, water solubility and non-toxic nature leads to many possible pharmaceutical and biomedical applications.

The main goal of this work is to study the electrical properties of PVA gels and use the results to obtain information about relaxation and structure of the gels. Another aim is to see how CNTs affect the properties and structure of the PVA cryogels. The results will give us information that may be useful in applications involving electric fields, such as magnetic resonance imaging and electronic devices. We also investigated two different ways to control the electrical conductivity of our PVA materials: changing the number of freeze-thaw cycles and adding carbon nanotubes.

In Chapter 2, we present the theoretical background of dielectric permittivity and the measurement technique. Chapter 3 describes the materials and the instruments used in this work. We present the dielectric behaviour of PVA and PVA nanocomposites in Chapter 4 as results of our work. Finally, Chapter 5 contains a discussion and summarizes our conclusions.

Chapter 2

Theory

2.1 Overview

In this Chapter, we present the theoretical background of dielectric spectroscopy. We first define dielectric materials then discuss their properties. We then introduce the complex permittivity and discuss the theory of dielectric spectroscopy.

2.2 Dielectric materials

Materials can be divided into three categories based on their electrical conductivity: conductors, semiconductors and insulators. The conductivity of a material can be explained using band theory. According to band theory, the valence band is the highest energy band that is completely filled with electrons and the conduction band is the lowest empty or partially filled band. The energy difference between the highest occupied level and the lowest unoccupied level is called the band gap E_g. In conductors, the conduction band is partially filled, so the band gap is zero, allowing electrons in the highest occupied levels to easily move into unoccupied states, resulting in an electric current when an external voltage is applied. In semiconductors, the band gap is non-zero, but small enough that a few electrons can be promoted to the conduction band thermally or by direct photon absorption. On the other hand, in insulators the

energy gap is much higher than the thermal energy, and the probability of a thermally excited electron crossing the band gap is very small.

Dielectric materials can be categorized as insulators, with band gap typically above 3 eV. These materials respond to an external electric field by polarization, but their electrical conductivity is very small because there are very few electrons in the conduction band.

2.2.1 Dielectric polarization

Some molecules have a permanent dipole moment even though their net charge is zero. The water molecule is one example. If a dielectric material containing molecular dipoles is in equilibrium with no applied electric field, the dipoles are oriented randomly. When a dielectric material is exposed to an external electric field, the field exerts a torque on the dipoles causing them to reorient in the field direction. The relative positions of the electrons and positive nuclei of non-dipolar materials shift slightly from their equilibrium positions when exposed to an electric field thus inducing a dipole moment. These processes result in what is called dielectric polarization.

Figure 2.1 explains the permanent dipole moment of water. The dipole moment exists due to the different electronegativities of hydrogen and oxygen. The dipole moment of water is 6.2×10^{-30} C m.

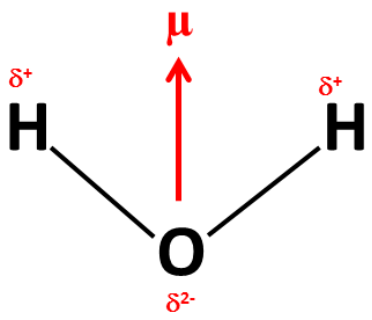

Figure 2.1: Schematic of the permanent dipole moment of water where δ^+ and δ^{2-} represent the relative electronegativities of hydrogen and oxygen respectively, and μ is the total dipole moment of the water molecule.

Figure 2.2(a) shows a dielectric material placed inside a parallel-plate capacitor with no applied electric field. The molecules are in equilibrium, and there is no net polarization. When an external electric field is applied across the capacitor, the relative positions of the electrons and positive ions change, as shown in Fig. 2.2(b). This induces an electric field inside the material that is opposite to the external electric field. The strength of the total field inside the material is the sum of the external field and the induced field, and it depends on the polarizability of the material.

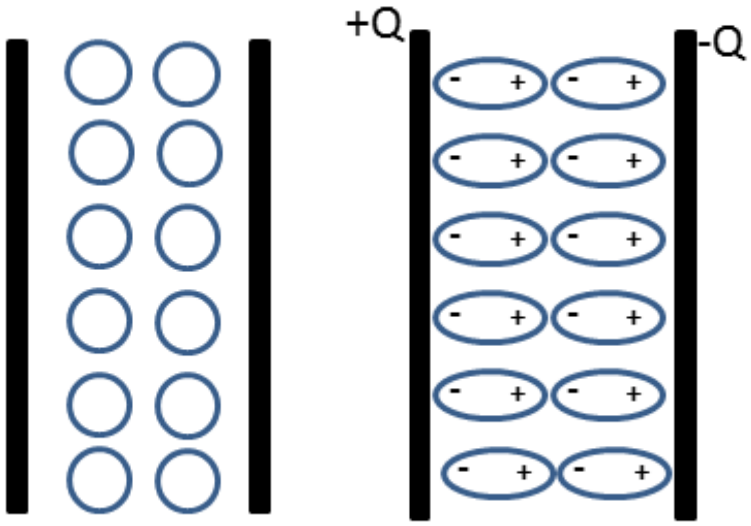

(a) (b)

Figure 2.2: A dielectric material in a parallel-plate capacitor (a) with no external electric field and (b) in an applied field. In (a), the electrons and positive nuclei are in equilibrium, and there is no net polarization. When the capacitor is charged, the applied field induces polarization in the dielectric, which in turn leads to an induced field in the dielectric.

2.3 Theory of dielectric spectroscopy

In dielectric spectroscopy, we study the influence of an alternating electric field on materials. Both a frequency domain and time domain measurement can be done. In the frequency domain, experiments are carried out with a sinusoidally alternating field, and the frequency is varied. In time-domain experiments, the field is changed suddenly, and the response is studied as a function of time. In our experiments, we use the frequency-domain approach.

2.3.1 Electric susceptibility and permittivity

Consider a capacitor that has a capacitance C_0 under vacuum and C when filled with a dielectric material. The electric susceptibility χ is defined by

$$\chi = \frac{C - C_0}{C_0}. \tag{2.1}$$

The electric permittivity ε is defined as

$$\varepsilon = \frac{C}{C_0}. \tag{2.2}$$

From equations 2.1 and 2.2, we obtain the relationship between susceptibility and permittivity

$$\chi = \varepsilon - 1. \tag{2.3}$$

The susceptibility is proportional to the material's polarizability. The polarization **P** is a vector that is related to the dipole moment in a unit volume of a dielectric material. The polarization vector of a dielectric material in an electric field **E** can be written as

$$\mathbf{P} = \chi \varepsilon_0 \mathbf{E}, \tag{2.4}$$

where ε_0 is the vacuum permittivity. By Equations (2.3) and (2.4)

$$\begin{aligned} \mathbf{P} &= (\varepsilon - 1)\varepsilon_0 \mathbf{E} \\ &= \varepsilon\varepsilon_0 \mathbf{E} - \varepsilon_0 \mathbf{E} \end{aligned}$$

$\varepsilon_0 \varepsilon \mathbf{E}$ is called the electric displacement **D** in the material. Then

$$\mathbf{P} = \mathbf{D} - \varepsilon_0 \mathbf{E}. \tag{2.5}$$

In a time varying electric field, $E(t) = E_0 \cos \omega t$, the polarization and the electric displacement **D** cannot follow the electric field exactly due to viscosity of the medium and the inertia of the electric charges. This causes the polarization vector to lag the electric field. As a result of this delayed response, there is a phase difference δ between the external electric field and the polarization and displacement vectors. The magnitude of the electric displacement field can be expressed as

$$D = D_0 \cos(\omega t - \delta). \tag{2.6}$$

Expanding the cosine function,

$$D = D_0 \cos \delta \cos \omega t + D_0 \sin \delta \sin \omega t. \tag{2.7}$$

We can introduce the complex permittivity

$$\varepsilon(\omega) = \varepsilon'(\omega) - i\varepsilon''(\omega), \tag{2.8}$$

where the real and imaginary parts of the permittivity are defined by [12]

$$\varepsilon' = \frac{D_0 \cos \delta}{\varepsilon_0 E_0} \tag{2.9}$$

$$\varepsilon'' = \frac{D_0 \sin \delta}{\varepsilon_0 E_0}. \tag{2.10}$$

The dielectric loss tangent or dissipation factor $\tan \delta$ is defined using Equations (2.9) and (2.10) as

$$\tan \delta = \frac{\varepsilon''}{\varepsilon'}. \tag{2.11}$$

The electrical conductivity of a dielectric material can be written as

$$\sigma(\omega) = \varepsilon_0 \varepsilon'' \omega. \tag{2.12}$$

$\varepsilon(\omega)$ is related to the complex impedance, which can be explained using a simple circuit as shown in Fig. 2.3, consisting of a resistor R and a capacitor C.

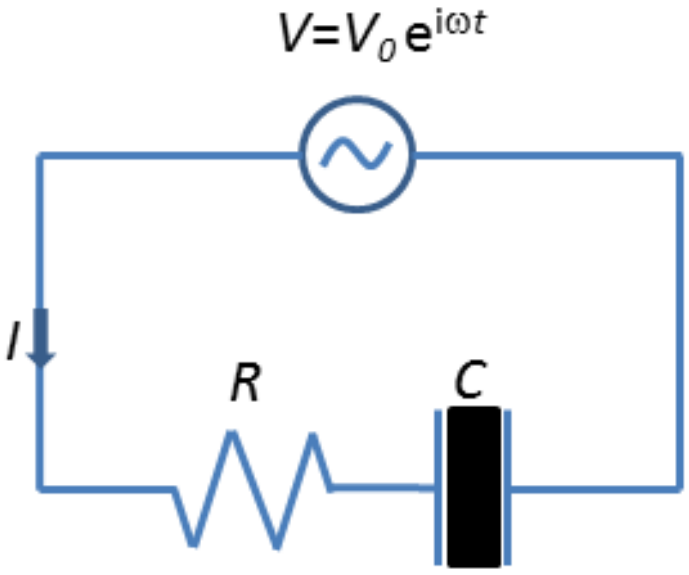

Figure 2.3: A RC circuit used to explain complex impedance where R is a resistor, C is a capacitor, I is current through the circuit and V is alternating voltage.

The equivalent impedance of the circuit can be expressed as

$$Z = R + \frac{1}{i\omega C}$$

or

$$Z = R - \frac{i}{\omega \varepsilon C_0}. \tag{2.13}$$

Equation 2.13 shows that the real part of the impedance represents the resistance of the circuit which causes dissipation of electrical energy. On the other hand, the imaginary part is related to the capacitance, which stores electrical energy. We can use this to understand the physical meaning of the real and imaginary parts of the permittivity by analysing the circuit shown in Fig. 2.4, which consists of a capacitor filled with a dielectric material with frequency-dependent

dielectric properties.

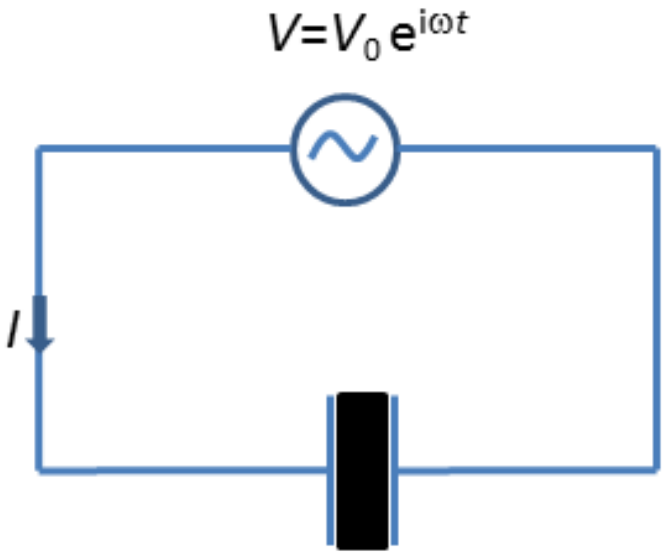

Figure 2.4: A capacitor filled with a dielectric material with a time varying voltage is applied across it.

The current through the capacitor is

$$\begin{aligned} I &= \varepsilon C_0 \frac{dV}{dt} \\ &= i\omega\varepsilon C_0 V \end{aligned}$$

The impedance of the capacitor is then

$$\begin{aligned} Z &= \frac{V}{I} \\ &= \frac{1}{i\omega\varepsilon C_0} \end{aligned} \tag{2.14}$$

Since $\varepsilon = \varepsilon' - i\varepsilon''$, then

$$\begin{aligned} Z &= \frac{1}{i\omega(\varepsilon' - i\varepsilon'')C_0} \\ &= \frac{1}{i\omega\varepsilon' C_0 + \omega\varepsilon'' C_0} \\ &= \frac{\varepsilon''}{\omega C_0(\varepsilon'^2 + \varepsilon''^2)} - \frac{i\varepsilon'}{\omega C_0(\varepsilon'^2 + \varepsilon''^2)}. \end{aligned} \tag{2.15}$$

As in Eq. (2.13), the first term on the right hand side of Eq. (2.15) represents the resistive part and the second term represents the capacitive part of the response of the dielectric material. The imaginary part of the permittivity is thus related to energy dissipation and the real part to energy storage in the material.

2.3.2 Dielectric measurement techniques

Generally, the complex impedance is measured and the dielectric function is derived from the complex impedance. From Eq. (2.14), the dielectric function can be expressed as

$$\varepsilon(\omega) = \frac{1}{i\omega Z(\omega) C_0}. \tag{2.16}$$

Different techniques are used to measure the complex impedance, depending on the frequency range of interest [13]. Frequency response analysis is commonly used for frequencies below 10 MHz. Figure 2.5 is a schematic circuit diagram illustrating this technique. The material being studied is placed in a capacitor. Two phase-sensitive voltmeters U_2 and U_1 are used to measure the voltages across a standard resistor R and the series combination of R and the experimental sample.

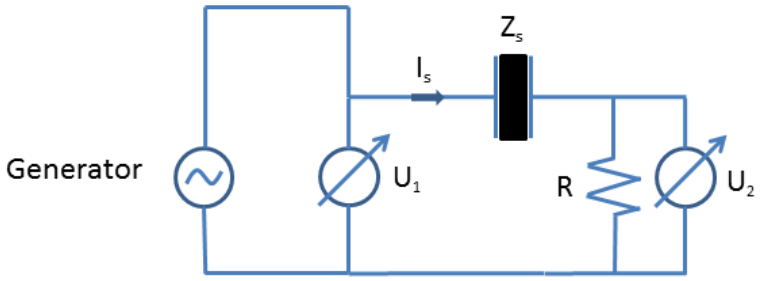

Figure 2.5: Schematic of measuring impedance using two vector voltmeters.

The impedance of the dielectric material in the capacitor can be written as

$$Z_s(\omega) = \frac{U_s(\omega)}{I_s(\omega)} \tag{2.17}$$

where $U_s(\omega)$ and $I_s(\omega)$ are the potential difference across the capacitor and current through the capacitor, respectively. Then

$$Z = \frac{U_1(\omega) - U_2(\omega)}{I_s(\omega)}$$

where $I_s = U_2(\omega)/R$. Then

$$Z = R\Big[\frac{U_1(\omega)}{U_2(\omega)} - 1\Big]. \tag{2.18}$$

The Solartron Materials Test System (MTS) used in our experiment uses a similar technique to measure the sample's impedance. Its schematic is shown in Fig. 2.6.

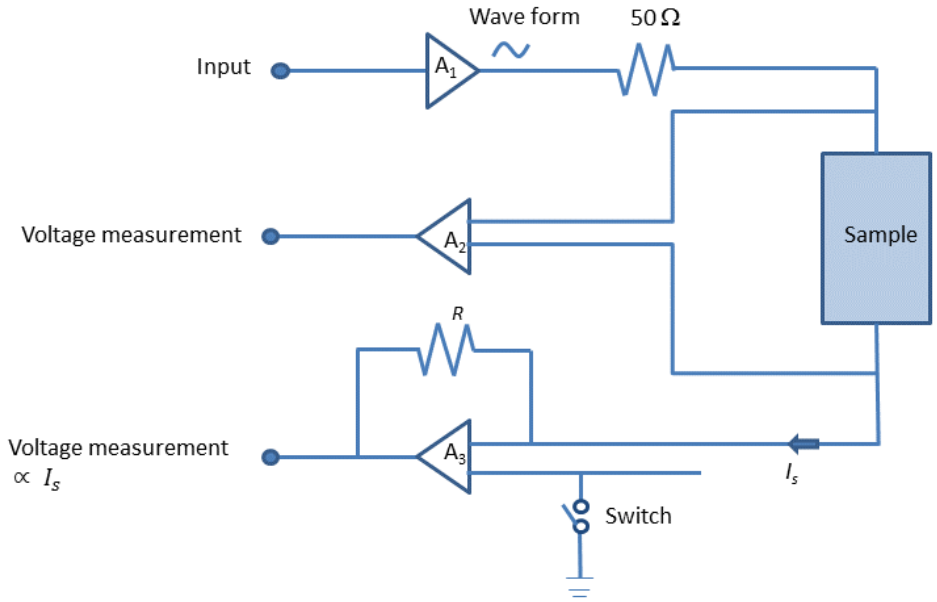

Figure 2.6: Schematic of the impedance measuring technique used in the Solartron MTS. A_1, A_2 and A_3 are the gains of the amplifiers shown.

An input signal is applied through the A_1 amplifier. The resulting voltage across the sample V_s is measured after the A_2 amplifier. The current through the sample I_s is calculated from the output voltage of the A_3 amplifier. The two voltage signals are input to a frequency response analyzer (FRA). The FRA calculates the phase angles and peak voltages of the two signals. Take the peak voltage and the phase angle of the signal sent through the A_2 to be V_2 and θ_2, respectively, and the corresponding values for the signal sent through the A_3 to be V_3 and θ_3. Then the peak voltage across the sample V_{sp} is

$$V_{sp} = \frac{V_2}{A_2}. \tag{2.19}$$

The peak current through the sample I_{sp} is

$$I_{sp} = \frac{V_3}{A_3 R}. \tag{2.20}$$

The complex impedance Z can then be written as

$$Z = \frac{V_{sp}}{I_{sp}} e^{i(\theta_2 - \theta_3)}. \tag{2.21}$$

The complex permittivity is then calculated using Eq. 2.16.

2.3.3 Dielectric relaxation

When a dielectric material is exposed to an electric field, the dipoles in the medium tend to align with the applied field in equilibrium. The dipoles randomize again after the field is removed, resulting in zero net polarization. This randomization process is known as dielectric relaxation. The characteristic time taken to reach the new equilibrium state is referred as the dielectric relaxation time, τ. The relaxation process depends on molecular structure, as well as on temperature, pressure, viscosity, and inertia of the dipoles, etc. There might be more than one relaxation process and corresponding time in some materials, depending on material morphology.

Debye [12, 14] developed a theory to explain the complex dielectric function and the relaxation process in gases and dilute solutions by assuming no interactions between molecular dipoles and an exponential approach to the equilibrium state. Debye's equation for $\varepsilon(\omega)$ is

$$\varepsilon(\omega) = \varepsilon_\infty + \frac{\varepsilon_s - \varepsilon_\infty}{1 + i\omega\tau}, \tag{2.22}$$

where ε_s and ε_∞ are the static and infinite frequency permittivities, and ω is the angular frequency of the electric field. The real and imaginary parts of this equation can be written as

$$\varepsilon'(\omega) = \varepsilon_\infty + \frac{\varepsilon_s - \varepsilon_\infty}{1 + \omega^2\tau^2} \tag{2.23}$$

and

$$\varepsilon''(\omega) = \varepsilon_\infty + \frac{\varepsilon_s - \varepsilon_\infty}{1 + \omega^2\tau^2}\omega\tau, \tag{2.24}$$

so that the loss tangent is

$$\begin{aligned} \tan\delta &= \frac{\varepsilon''(\omega)}{\varepsilon'(\omega)} \\ &= \frac{(\varepsilon_s - \varepsilon_\infty)\omega\tau}{\varepsilon_s + \varepsilon_\infty\omega^2\tau^2}. \end{aligned} \tag{2.25}$$

The dielectric loss tangent $\tan\delta$ is a peaked function which can be used to find the relaxation time τ. Setting the first derivative of $\tan\delta$ in Eq. 2.25 to zero, the relaxation time can be written as

$$\tau = \frac{1}{\omega_{max}}\sqrt{\frac{\varepsilon_s}{\varepsilon_\infty}} \tag{2.26}$$

where ω_{max} is angular frequency of the peak in $\tan\delta$.

As an example, ε', ε'' and $\tan\delta$ were calculated from Debye's equation supposing $\varepsilon_\infty = 5$ and $\varepsilon_s = 80$. The results are plotted as functions of angular frequency in Figs. 2.7, 2.8, and 2.9.

Figure 2.7 shows the real part of the Debye permittivity versus angular frequency. The center of the sudden decrease in ε' occurs at a angular frequency equal to $\frac{1}{\tau}$.

Equation (2.24) for the dielectric loss ε'' is a peaked function as shown in Fig. 2.8. The reciprocal of the peak frequency gives τ, the relaxation time of the sample.

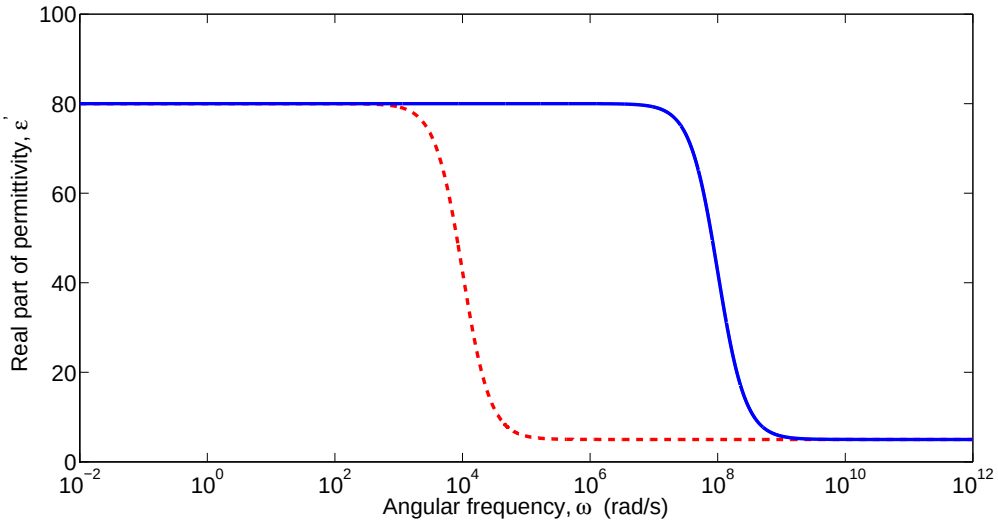

Figure 2.7: Real part of the Debye's permittivity versus angular frequency. The red dashed line shows ε' when $\tau = 10^{-4}$ s and the blue line when $\tau = 10^{-8}$ s. Here $\varepsilon_s = 80$ and $\varepsilon_\infty = 4$.

The position of the dielectric loss peak varies with the relaxation time as shown in Fig. 2.8.

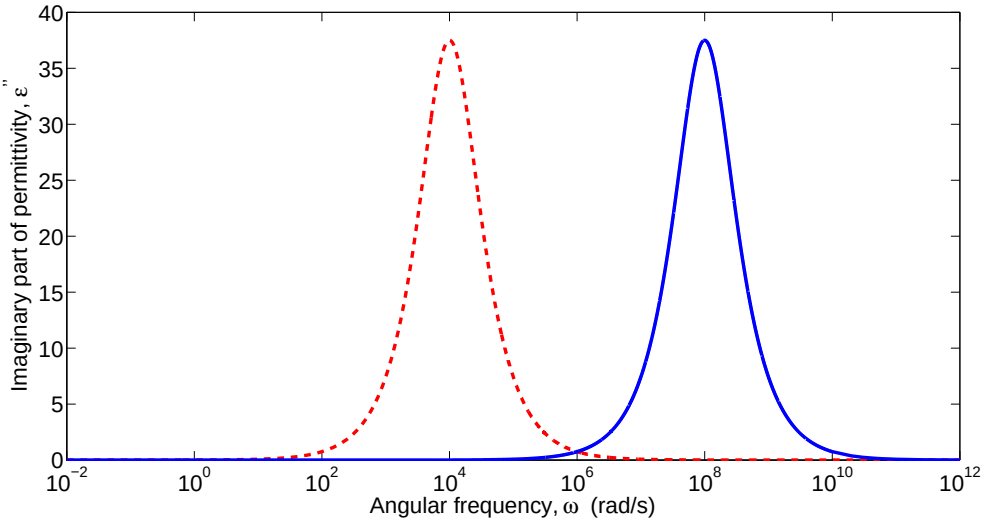

Figure 2.8: Imaginary part of the Debye's permittivity versus angular frequency. The red dashed line shows ε'' when $\tau = 10^{-4}$ s and the blue line when $\tau = 10^{-8}$ s. Here $\varepsilon_s = 80$ and $\varepsilon_\infty = 4$.

Figure 2.9 shows the dielectric loss tangent of the Debye permittivity versus angular frequency. Comparing Figs. 2.8 and 2.9, it can be seen the peak frequency (ω_{max}) has shifted by a factor $\sqrt{\frac{\varepsilon_s}{\varepsilon_\infty}} = 4$ in the dielectric loss tangent spectrum.

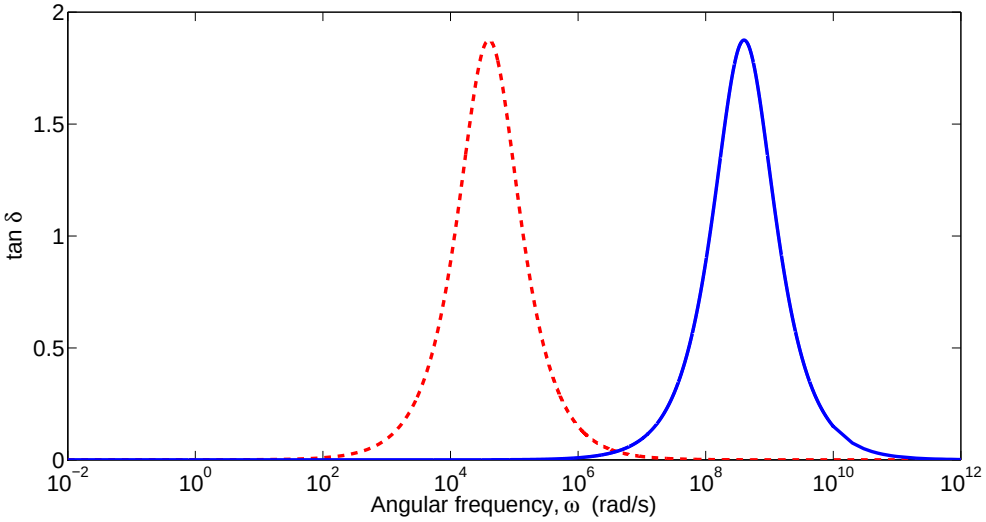

Figure 2.9: Dielectric loss tangent from the Debye permittivity versus angular frequency. The red dashed line shows $\tan\delta$ when $\tau = 10^{-4}$ s and the blue line when $\tau = 10^{-8}$ s. Here $\varepsilon_s = 80$ and $\varepsilon_\infty = 4$.

The dielectric behaviour of complex materials such as polymer composites cannot be explained by the simple Debye model due to interactions between dipoles and the presence of more than one relaxation process. Several researchers have modified the Debye equation to model the behaviour of these materials. Some models involve adding more relaxation terms to the Debye model [15]. Another modified Debye model is the Cole-Cole model, which has been used to fit the dielectric response in polymers. The Cole-Cole equation for the dielectric permittivity is [16]

$$\varepsilon(\omega) = \varepsilon_\infty + \frac{\varepsilon_s - \varepsilon_\infty}{1 + (i\omega\tau)^{1-\alpha}}, \tag{2.27}$$

where the exponent α is between 0 and 1. When α =0, the Cole-Cole equation reduces to the Debye model. Havriliak and Negami postulated a relaxation function that is a modification of the Cole-Cole equation. The Havriliak-Negami equation [17] is

$$\varepsilon(\omega) = \varepsilon_\infty + \frac{\varepsilon_0 - \varepsilon_\infty}{[1 + (i\omega\tau)^{1-\alpha}]^\beta}, \tag{2.28}$$

where the exponent β is between 0 and 1. The Havriliak-Negami equation has itself been modified [18] by adding an extra relaxation term and a direct current term. The modified Havriliak-Negami equation is

$$\varepsilon(\omega) = \varepsilon_\infty + \frac{\Delta\varepsilon_{EP}}{(1 + i\omega\tau_{EP})^\beta} + \frac{\Delta\varepsilon_\alpha}{[1 + (i\omega\tau_\alpha)^\delta]^\gamma} + \frac{\sigma_{dc}}{i\omega\varepsilon_0}, \tag{2.29}$$

where EP represents electrode polarization, α denotes Debye relaxation, and σ_{dc} is the D.C. conductivity. The modified Havriliak-Negami equation has been used to interpret the dielectric response of ice and water under pressure [18].

2.3.4 Electrode polarization

When materials are exposed to an electric field, electrical charges can be accumulated at interfaces between two materials or between two regions within a material. This phenomenon is called interfacial polarization [19]. When the charge accumulation happens at an interface between an electrode and a dielectric material, the interfacial polarization is known as electrode polarization.

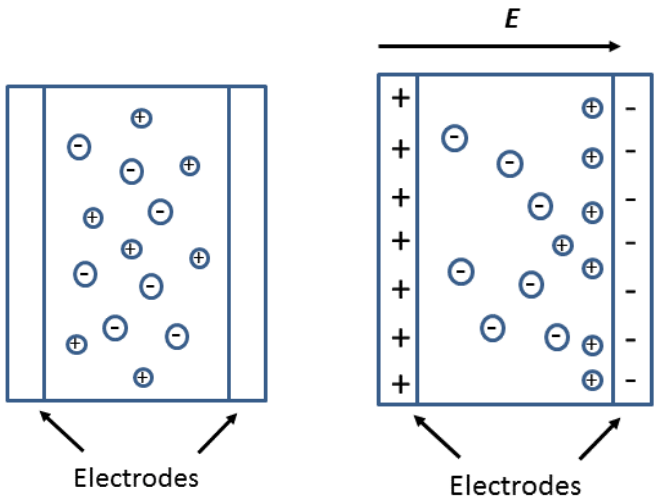

(a) (b)

Figure 2.10: A dielectric material with equal number of positive and negative ions. The positive ions are more mobile than the negative ions. (a) No external electric field and (b) in an applied field.

Materials may contain various mobile charge carriers such as electrons, holes, or ionized ions. The dielectric material shown in Fig. 2.10(a) has an equal number of positive and negative ions. The positive ions, which we assume are more mobile, migrate and pile up at the negative electrode when the external electric field is applied, as shown in Fig. 2.10(b). If the negative ions were also mobile, there would be another charge accumulation near the positive electrode.

From Eq. (2.2), permittivity of a dielectric material can be written as

$$\begin{aligned} \varepsilon &= \frac{C}{C_0} \\ &= \frac{Q}{Q_0}, \end{aligned} \tag{2.30}$$

where Q_0 is charge on the capacitor under vacuum and Q when it is filled with a dielectric material. When electrode polarization exists, the positive ions at the interface between the dielectric material and the negative electrode attract more electrons to the electrode. This additional charge causes the permittivity of the material to increase in accordance with in Eq. (2.30).

The electrode effect is dominant at low frequencies as a sufficient time is available for the charge accumulation. This causes the permittivity to increase at low frequencies. Electrode polarization is accommodated by the third term in the modified Havriliak-Negami model [18].

2.3.5 Dielectric relaxation in polymers

A polymer material is a collection of polymer chains, and a polymer chain is made of repeated monomers. This means that the net dipole moment per unit volume, or polarization vector, of a polymer depends on molecular dipoles in the monomer and the configuration of the individual polymer chains, summed over the entire system. The polarization of a polymer can be written

as [13]

$$\vec{\mathbf{P}} = \frac{1}{V} \sum_{allchains} \sum_{chain} \sum_{repeating\,unit} \vec{\mu_{\mathbf{i}}} \tag{2.31}$$

where μ_i is dipole moment.

As polarization can be due to dipoles on all these levels, and as molecular motions in a polymer can have a broad range of time and length scales, different motional processes can affect the reorientation of the dipole moment. As a result, one expects more than one dielectric relaxation process in a polymer. Each process is typically characterized by a peak in the dielectric loss spectrum and a step-like decrease in ε'. Dielectric relaxation can be also studied taking measurements at a fixed frequency as a function of temperature. In this case, a relaxation process gives a peak in ε'' versus temperature and a step-like decrease in ε' versus temperature.

Two types of relaxation processes, known as α relaxation and β relaxation, are observed in most amorphous polymers. α relaxation is also known as principal relaxation and β as the secondary relaxation. The well-accepted explanation for the β relaxation is variation of the local dipole vector movement of small regions of the main polymer chain, and/or rotations of side groups [13]. The β relaxation process can be observed at higher frequencies as the localized fluctuations relax in short times. In contrast, the α relaxation is caused by reorientation of entire chains or longer chain segments. As these motions happen over larger length scale, the α relaxation process also depends on interactions between chains. The α relaxation is seen at low frequency, as more time is needed to reorient larger regions. Both relaxation process are temperature sensitive.

Chapter 3

Experiment

3.1 Overview

In this Chapter, we describe the apparatus and procedure used in our dielectric experiments, and the materials studied. We first introduce the dielectric spectrometer which was used for our experiments. Its operation and the way it was used to take measurements over a large temperature range are explained. We then discuss the preparation of the PVA-based samples studied in this work.

3.2 Dielectric spectrometer

The measuring system consists of several components which together comprise the dielectric spectrometer. Fig. 3.1 is a photograph of the spectrometer in our lab, showing the main components. These are the material test system (MTS), the cryostat and cooling system, and the temperature controller.

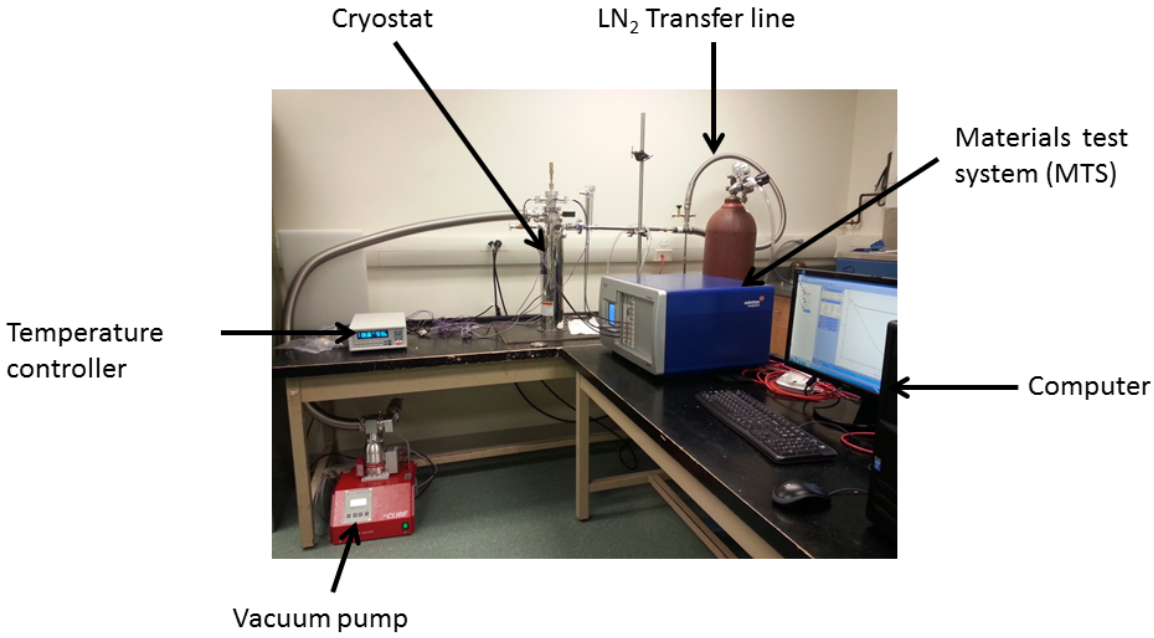

Figure 3.1: Altogether, the MTS, the cryostat and cooling system, and the temperature controller is the called dielectric spectrometer. The MTS and the temperature controller commands are given through the computer.

The blue box in Fig. 3.1 is a Solartron Modulab (MTS) [20], which contains the electronics used. The MTS communicates with the Modulab MTS computer software running on the lab computer through an ethernet connection. The MTS can be used to perform several measurements. For example, in an open-circuit measurement, the decay of the voltage across a sample with time is measured after the sample has been polarized by an external electric field. Direct current measurements involve applying a voltage across the sample and measuring the resulting constant current.

In our research, we mainly used the instrument to perform voltage-controlled impedance measurements with a constant AC voltage amplitude. The DC offset voltage was fixed at 0 V to avoid dielectric polarization. The MTS generates a sinusoidal voltage signal in the frequency range from 10 μHz to 1 MHz, which is applied across the sample cell. The resulting current is measured, and the software calculates the desired dielectric quantities.

The stainless steel cylinder in Fig. 3.1 is the cryostat. The sample cell(capacitor) is held in the cryostat, and the desired sample temperature can be reached by controlling heaters inside the cryostat as well as the flow of liquid nitrogen (LN) through it.

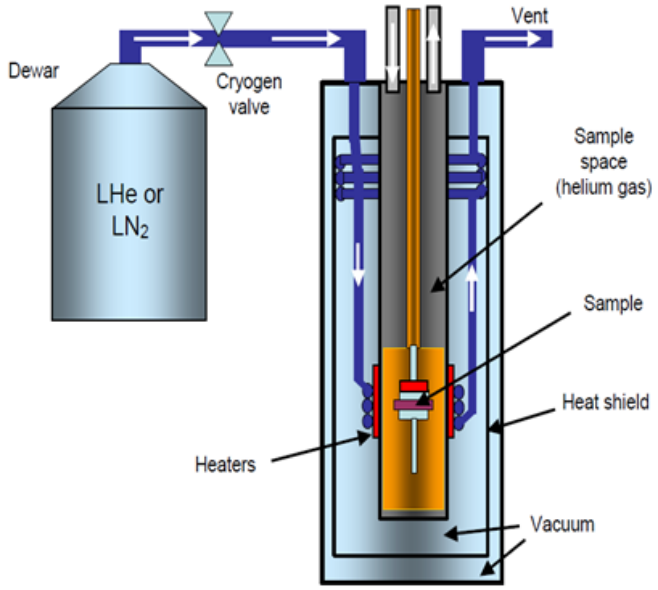

Figure 3.2: A cross section of the cryostat showing the main components inside the cryostat and their organization [21].

Figure 3.2 [21] shows the design of the cryostat. The cryostat consists of three concentric stainless steel cylinders. The space between the outer two cylinders is a vacuum jacket. It must be evacuated to a pressure 5×10^{-4} Torr or less using a turbo pump prior to every experiment to reduce cryogen consumption and heat transfer with the environment. The space inside the inner cylinder is pumped down to close to 10^{-3} Torr, after which helium exchange gas is introduced at a pressure 1 PSI above atmospheric pressure to ensure good heat transfer to the sample. Liquid nitrogen flows from a storage dewar through a transfer line and tubes in the space between the middle and inner cylinders to cool the system. The outer jacket of the transfer line is also pumped down to 5×10^{-4} Torr to reduce cryogen consumption. The sample is held between the copper plates of a parallel-plate capacitor in the inner cylinder of the cryostat. There are two heaters in the cryostat. One is mounted near the sample holder to heat the sample when needed and the other is placed on the outer surface of the inner cylinder to heat the area surrounding

the capacitor. Two thermocouples are installed in the cryostat. One is at the sample holder to measure the sample's temperature, and the other is at the outer surface of the inner cylinder.

In our experiments, we studied the dielectric properties of our samples as a function of temperature. Liquid nitrogen is used as a cryogen to cool the sample below ambient temperature. As the boiling point of liquid nitrogen is 77 K, it would be possible to explore the dielectric properties of the samples to temperatures as low as 77 K. The system can also be heated to 600 K. However, we were interested in temperatures between 200 K and 300 K. The temperature of the sample is controlled by a Lake Shore Model 335 Cryogenic Temperature Controller [22] which balances the cooling due to the cryogen against heating from the heaters in the cryostat to maintain the desired temperature. The sample temperature can be controlled to 0.01 K accuracy using the temperature controller.

3.3 Materials

3.3.1 Polyvinyl alcohol (PVA)

Figure 3.3(a) shows the structure of a vinyl monomer. Here, R denotes a functional group: for example, if the R group is hydrogen, the monomer is ethylene and, after polymerization as in Fig. 3.3(b), becomes polyethylene, which is a well known plastic.

The polymer used in our experiment is PVA. The repeating unit or monomer of PVA is vinyl alcohol (CH_2=CHOH), which can be represented in Fig. 3.3 with R being a hydroxyl group. PVA is not made simply by polymerization of vinyl alcohol due to the instability of the vinyl alcohol monomer. Instead, polyvinyl acetate (PVAc) is made by polymerization of vinyl acetate monomers (CH_2=CHO–$COCH_3$), followed by hydrolysis to make PVA [1].

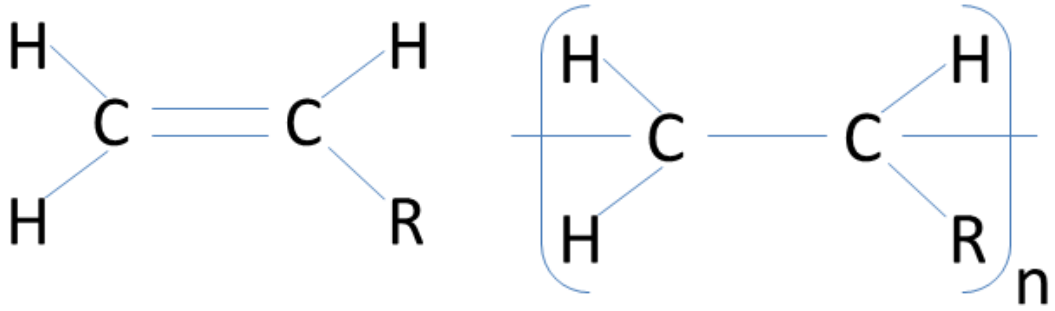

(a) Vinyl monomers (b) Vinyl polymers after the polymerization

Figure 3.3: A vinyl monomer and its corresponding vinyl polymer.

The vinyl acetate monomer can be represented by Fig. 3.3(a) with R being an acetate group (CH_3–CO_2–). Commercially, PVA is a co-polymer of PVA and PVAc, as PVAc can not completely be converted to PVA. The solubility and chemical properties of PVA depend on the degree of hydrolysis. For our research, white and odorless PVA powder with molar mass 89,000–98.000 g/mol and 99% hydrolyzation was purchased from Sigma-Aldrich Co.

3.3.2 PVA hydrogels

The hydrophilic OH groups on the polymer can form hydrogen bonds with water molecules, allowing it to dissolve. In the gel state, polymer crosslinking prevents the hydrogel from dissolving in water and polar solvents. Hydrogels can absorb and store large amounts of water through the hydrogen bonds. Hydrogels are used as biomaterials for drug delivery, wound covering materials, artificial dental materials, etc.

Crosslinking between polymer molecules can be physical or chemical. Chemical crosslinking is achieved by adding chemical agents to the polymer. For example, in rubber vulcanization, sulfur is added to natural rubber to chemically link the polymer molecules together. PVA can be chemically crosslinked by adding glutaraldehyde or formaldehyde [23]. There are

drawbacks to using chemically crosslinked hydrogels as biomaterials, however, as some of the agents used are toxic.

A polymer solution can be crystallized by changing temperature and aging. This is an example of physical crosslinking. Physical crosslinking of PVA can be achieved by micro-crystallization on cooling and thawing. When the temperature of PVA solution is decreased, the molecular motions of the polymer are also decreased and small regions of crystalline polymer can form. These crystallites act as crosslinks leading to the formation of a hydrogel. The degree of crosslinking depends on the concentration of PVA, the cooling and thawing times and the number of freeze-thaw cycles. As a result of this crosslinking, individual polymer chains combine to make larger branched polymers, as illustrated in Fig. 3.4. When the number of crosslinks is small, the number and length of the branched polymers are relatively small and the polymer is said to be in the sol state.

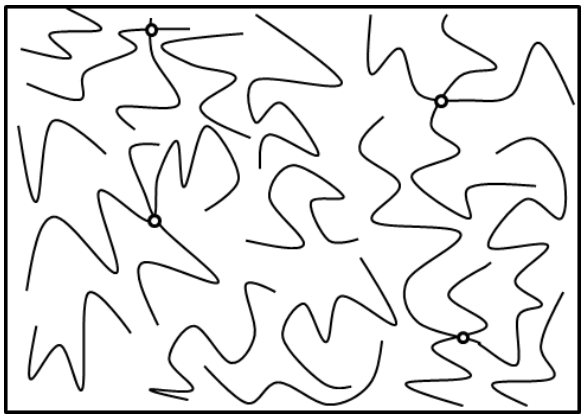

Figure 3.4: Polymer crosslinking. There are four crosslinks here shown as small circles. This can be considered as a sol state polymer.

When the crosslinking process continues via crystallization as the temperature decreases, more and larger branched polymers appear as the chains become more interconnected. At a certain temperature, the branched polymers span the sample, and the system undergoes a transition from the sol to the gel state as shown in Fig. 3.5 [4]. This transition temperature is called the gel point.

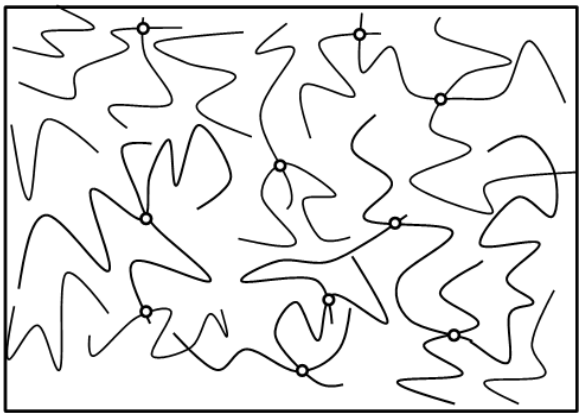

Figure 3.5: Schematic of PVA in gel state. More crosslinks exist due to further crystallization of PVA. Note that the system spanned by one crosslinked chain.

3.3.3 Carbon nanotubes

The exceptional mechanical and electrical properties of carbon nanotubes have brought much attention from researchers and industry. For example, their elastic modulus is 1.2 TPa, close to that of diamond, and their electrical conductivity can be similar to that of copper. Polymer-CNT nanocomposites have been made with a percolation threshold concentration as small as 1.4% by weight [5]. The enhancement of electrical and mechanical properties of polymer-based carbon nanotube composites are mainly dependent on the ability to create a homogeneous dispersion of CNT in the polymer and the purity of the CNTs. Carbon nanotubes in a dispersion tend to aggregate due to van der Waals forces between tubes. Single-walled carbon nanotubes (SWCNT) are often contaminated with impurities such as graphitic nanoparticles, amorphous carbon, and metal catalysts used in the CNT production.

For our work, the raw CNTs were purified following the chemical treatment described by Kazemi-Zanjani et al. [24]. Raw single walled carbon nanotubes (SWCNT) made by a plasma torch technique were purchased from Raymor Nanotech. 0.4 g of raw SWCNT were powdered using a spatula. The powder was put in a 2 L round-bottom flask and 1360 ml of 7 M nitric acid (HNO_3) was added in fume hood. The mixture was sonicated for 20 minutes to disperse

the CNTs. The mixture was then heated for four hours at 100 °C. The nitric acid is able to remove a large fraction of the amorphous carbon and metal catalysts [25]. A condenser on the flask recirculated the evaporated mixture back into the flask. The reaction was stopped after 4 hours by slowly adding 2 kg of ice. Damage to the CNTs by nitric acid was minimized by choosing a short reaction time [25]. Once the mixture reached ambient temperature, it was filtered through 0.2 μm filters, then water was added, and it was filtered again until the filtered water was neutralized (pH 7). As a final step, another 4 L of deionized water was added and the suspension filtered again to confirm the neutralization. The CNTs were then kept in a vacuum chamber for a few days to allow all water to evaporate. In addition to removing metallic crystals and amorphous carbon, the nitric acid treatment introduces carboxylic acid groups to the CNTs. Carbon nanotubes purified and functionalized in this way dispersed easily in water after sonication.

The length of the CNTs used in our research was between 0.3 μm and 4 μm, as supplied. The degree of polymerization n of our PVA is given by [4]

$$n = \frac{M}{M_{mon}} \tag{3.1}$$

where M is molar mass of PVA and M_{mon} is molar mass of the monomer, which in our case is 44 g/mol. Using M = 93500 g/mol, the degree of polymerization of PVA we used in this experiment is approximately 2125. The maximum end to end distance R of a PVA chain is [4]

$$R = 2nl\cos\frac{\theta}{2} \approx 0.4\ \mu m \tag{3.2}$$

where l=0.154 nm is the length of a C–C bond and $\theta = 108^\circ$ is the bond angle. Since the PVA chains will certainly not be fully extended, we can easily conclude that CNTs are much longer than the size of a single PVA molecule.

3.4 Sample preparation

3.4.1 Polyvinyl alcohol solution

Deionized water was heated to 90 °C on a hotplate, after which the required amount of PVA powder was added to get a PVA concentration of 12% by weight. The solutions were then stirred for three hours with a magnetic stirrer while maintaining the solution's temperature at 90 °C. The beaker was covered to prevent evaporation.

3.4.2 Polyvinyl alcohol hydrogels

A 12 wt% PVA solution prepared as above was transferred to molds made from aluminum plates 10 cm by 10 cm by 1.5 cm thickness, separated by a 2.5 mm thick teflon gasket. The sealed aluminum molds were immersed in a programmable PolyScience PP07R-40 circulating bath and subjected to a number of freeze-thaw cycles. Each cycle cooled the molds from 20 °C to –20 °C at a rate of 0.12 °C/min, then remained at –20 °C for two hours before warming back to +20 °C at the same ramp rate [9, 26]. The gels were then removed from the molds and cut into 25 cm diameter circles. Dielectric measurements were taken with the samples in between the copper electrodes of the measuring capacitor in the cryostat.

3.4.3 Polyvinyl alcohol/carbon nanotubes composites

Nanocomposite materials made from PVA with 0.1%, 0.5% and 1% CNT were made as follows. The desired amount of purified and dried CNTs was added to deionized water and sonicated for 5 hours to disperse them homogeneously in the water. This dispersion was then heated to 90 °C and PVA powder was added to give a PVA concentration of 12% by weight. The solutions were then stirred for three hours, maintaining the solution's temperature at 90 °C. The container was covered to prevent evaporation.

3.5 Procedure

The dielectric properties of PVA cryogel were measured in two ways. In the first, the cryogel samples made using the circulating bath were tested between 200 K and 300 K. Once the desired temperature was reached, it was maintained for 20 minutes to ensure that the sample temperature was stable and uniform before the Modulab MTS computer software was used to collect dielectric data. In the second method, a PVA solution was loaded into the sample cell and studied while it undergoes freeze-thaw cycles in the cryostat following the same steps in the thermal cycle as in the circulating bath. The complex permittivity of the nanocomposites was measured using the second of these experimental methods.

Chapter 4

Results

We present our experimental results in this chapter. The dielectric spectrometer was first tested by making measurements on a test circuit and samples of Teflon as a known dielectric material. Then we present results for the dielectric properties for water, PVA solution, PVA cryogel, and nanocomposites made by adding carbon nanotubes to a PVA solution. The results are interpreted in terms of existing models for the dielectric response.

4.1 Testing the spectrometer

As this was the first time the dielectric spectrometer was used in our group, the instrument was tested using a test module provided by Solatron Analytical and with Teflon discs. Both testing methods showed that the spectrometer worked as expected.

4.1.1 Test module

Figure 4.1 illustrates the electrical circuit of the test module, which consists of a standard 100 kΩ resistor connected in series with a 10 nF capacitor, and a 100 pF capacitor in parallel with the series combination. The points labelled General and Input in the figure were connected to the spectrometer, and the impedance and phase angle of the circuit were measured.

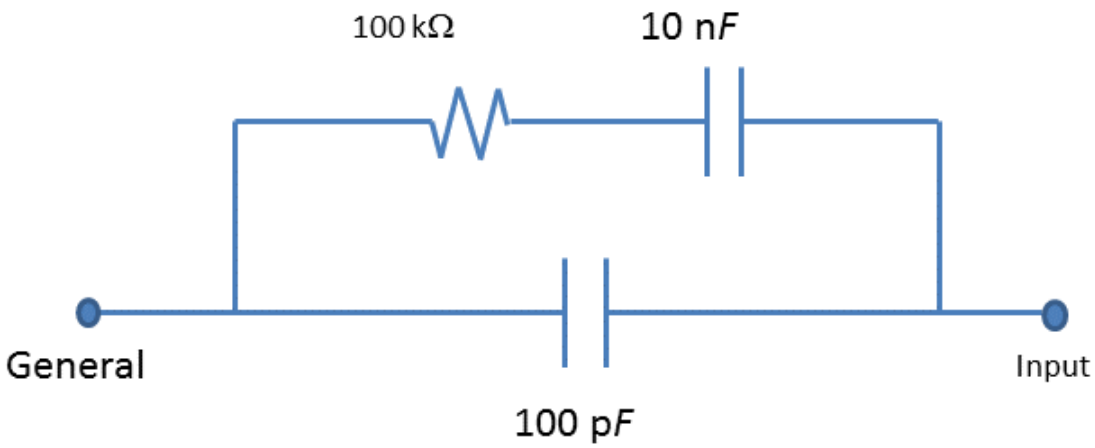

Figure 4.1: The electrical circuit of the test module which was used to test the spectrometer.

Considering the impedance of each component, the theoretical impedance of the circuit can be written as

$$Z = \frac{10^{15}}{\omega^2 + 1.02 \times 10^{10}} - i\frac{\frac{10^{10}}{\omega}(\omega^2 + 1.01 \times 10^8)}{\omega^2 + 1.02 \times 10^{10}}, \tag{4.1}$$

where ω is angular frequency. The phase angle θ of the electric circuit is given by

$$\begin{aligned} \tan\theta &= \frac{Im\{Z\}}{Re\{Z\}} \\ &= \frac{-10^{-5}}{\omega}(\omega^2 + 1.01 \times 10^8). \end{aligned} \tag{4.2}$$

Figure 4.2 shows the theoretical and experimental values of the absolute value of the impedance $|Z|$, and Fig. 4.3 shows the phase angle versus angular frequency. The experimental and theoretical values match extremely well, demonstrating that the spectrometer was working properly.

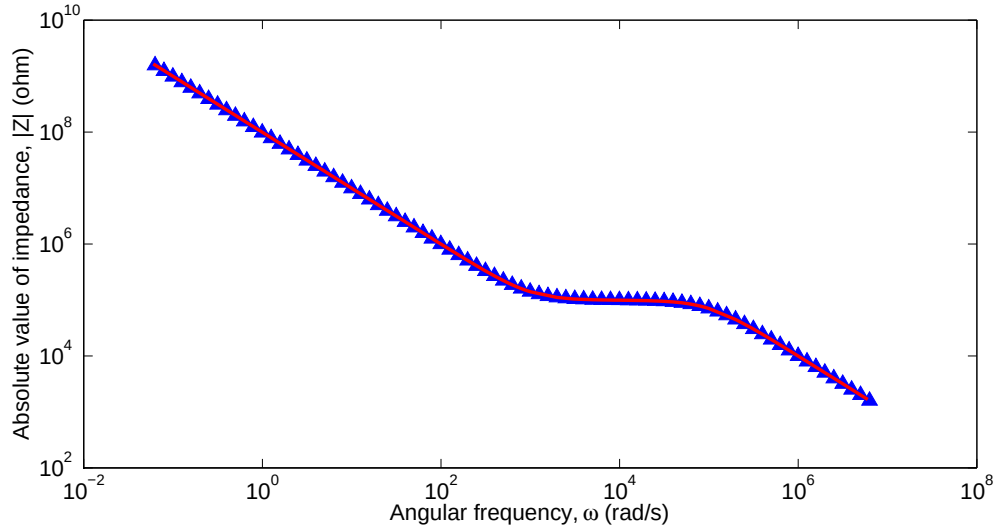

Figure 4.2: Theoretical and experimental values of absolute impedance of the test module versus angular frequency. The blue triangles represent measured absolute impedance and the red line shows the theoretical values calculated with Eq. (4.1).

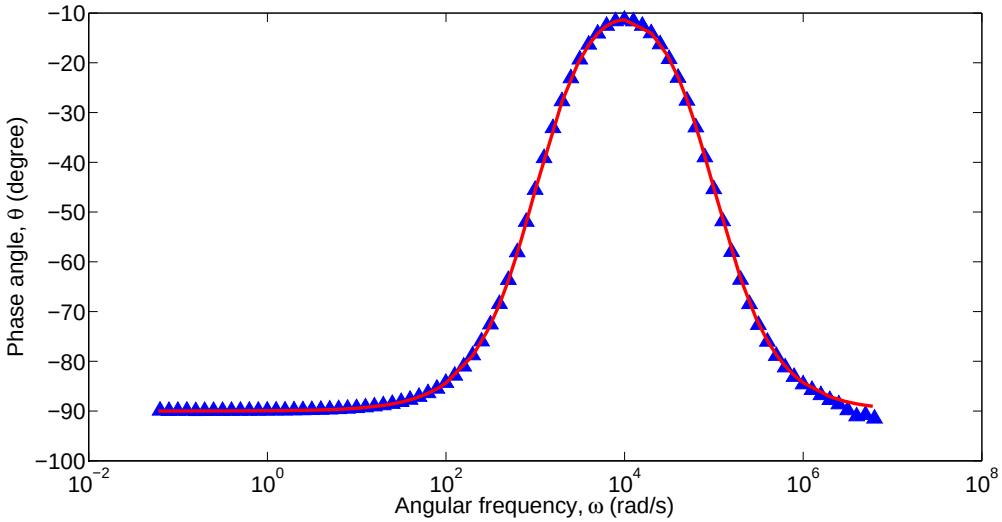

Figure 4.3: Theoretical and experimental values of phase angle versus angular frequency for the test module. The blue triangles represent measured data and the red line shows theoretical values calculated with Eq. (4.2).

4.1.2 Teflon

The relative permittivity of Teflon disks of two different thicknesses were measured by placing the samples between the electrodes of the measuring capacitor. The sample thicknesses were

0.50 mm and 0.75 mm and their diameters were selected as 25 mm so that the disks filled the electrode. Figure 4.4 shows that the dielectric constant is independent of thickness, as expected. The mean measured dielectric constant of 2.01± 0.03, where the uncertainty is estimated from the standard deviation of values in the figure, is in agreement with the literature value of 2.002 [27].

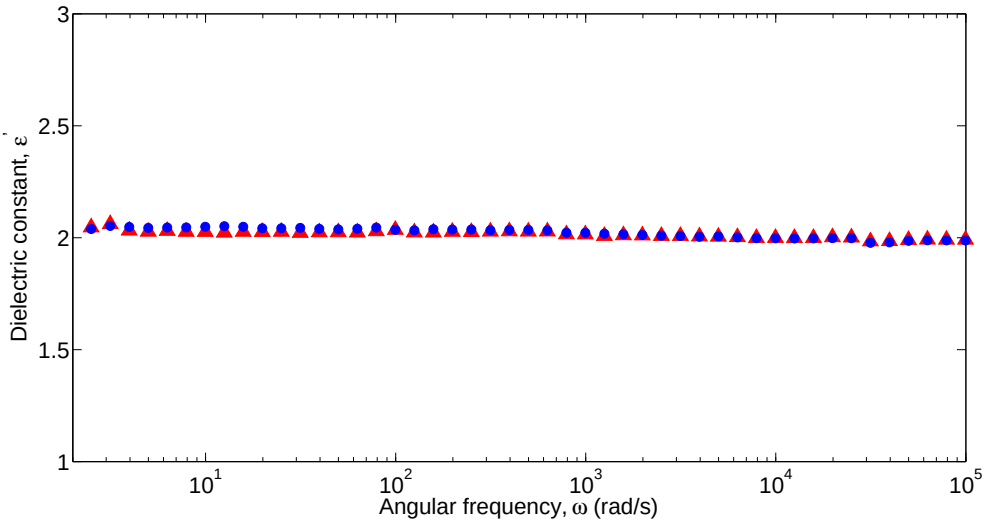

Figure 4.4: Permittivity of two different thicknesses of teflon at 293 K. The red triangles show data for a 0.5 mm thick sample and the blue dots for 0.75 mm thick.

As the two tests were successful, the spectrometer was used to measure the dielectric properties of PVA and its composites.

4.2 Results for water, PVA and PVA nanocomposites

PVA solutions, cryogels and nanocomposites were tested over a frequency range of 100 mHz to 1 MHz at different temperatures. As all the samples contain more than 87% water, the dielectric behaviour of water was studied first for comparison and to aid us in understanding the data for the PVA materials. PVA cryogels were tested using two different methods. In the first method, the samples were prepared by freeze-thaw cycles in a temperature-controlled bath, then tested in the cryostat. In the second method, data were taken while the sample underwent freeze-thaw

cycles in the cryostat itself. The dielectric data of nanocomposites with 0.1 wt%, 0.5 wt% and 1.0 wt% CNTs were taken while the samples were undergoing freeze-thaw cycles in the cryostat.

4.2.1 Dielectric properties of water

The dielectric response of water was studied at temperatures between 200 K and 300 K. The real and imaginary parts of the relative permittivity, ε' and ε'' are plotted in Figs. 4.5 and 4.6.

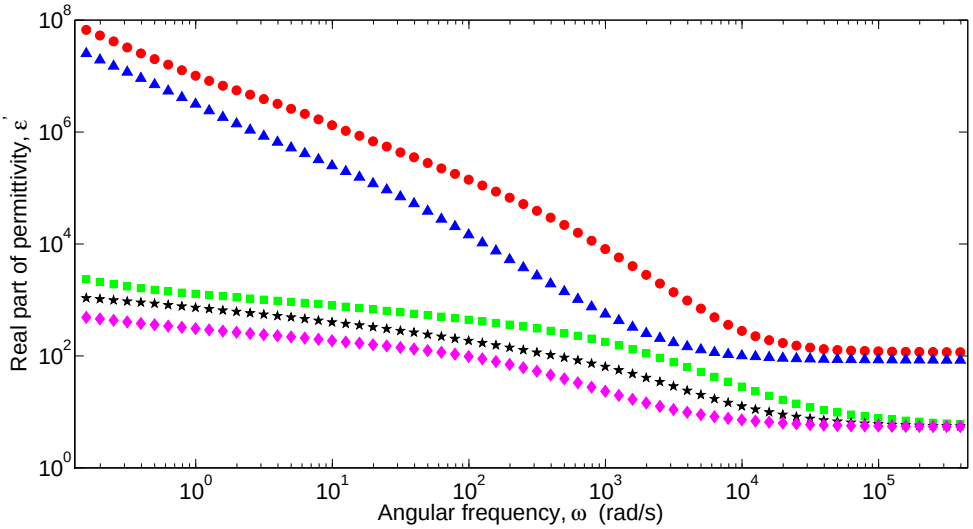

Figure 4.5: Real part of permittivity of water at different temperatures: red circles: 290 K, blue triangle: 275 K, green squares: 250 K, black pentagrams: 225 K and magenta diamonds: 200 K.

The real part of the permittivity increases at low frequencies as electrode effects become dominant. It shows a constant value at high frequencies due to dipole polarization. At high temperatures, the imaginary part does not show a relaxation peak as the relaxation time of liquid water is very short. For example, it is 9.6 ps at 293 K [15].

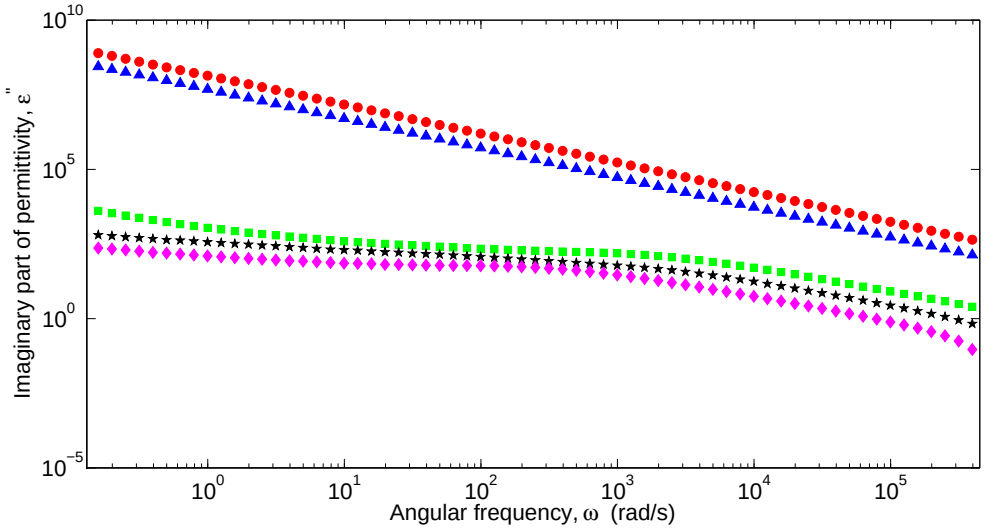

Figure 4.6: Imaginary part of permittivity of water at different temperatures: red circles: 290 K, blue triangle: 275 K, green squares: 250 K, black pentagrams: 225 K and magenta diamonds: 200 K.

Figures 4.5 and 4.6 show a few similar features. First, both the real and imaginary parts of the permittivity decrease when the temperature goes down. When temperature decreases, the kinetic energy of the water molecules also decreases proportionally to the absolute temperature while the viscosity of water increases. Both effects reduce the motion of the water dipoles. This leads to the reduction in both the real and imaginary parts of the permittivity. However the major differences between the data at 275 K and at 250 K are due to the water freezing as it cools.

Another similar feature is that the both parts of the permittivity increase when the frequency decreases. This can be explained by considering time available for the molecular dipoles to follow the field. At low frequencies, the dipoles have sufficient time to follow and align with the field, resulting in larger values of the permittivity.

Below the freezing point, the real part of the permittivity of water displays behaviour quite similar to the Debye model explained in Section 2.3.3. However, the expected Debye peak

in ε'' is barely visible in Fig. 4.6. More information about the dipolar relaxations in water at different temperatures can be obtained by looking at the dissipation factor or dielectric loss tangent.

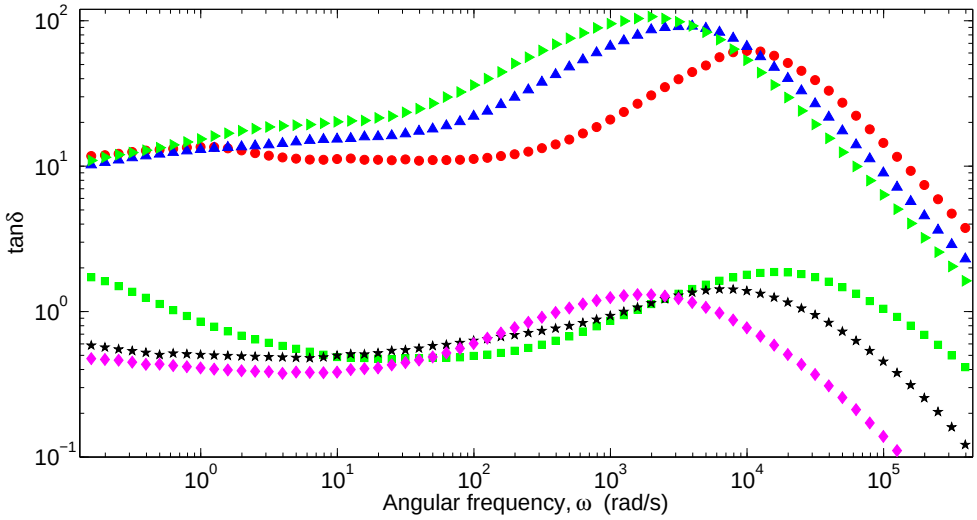

Figure 4.7: Dielectric loss tangent of water at different temperatures: red circles at 290 K, blue upwardly pointing triangles at 280 K, green right triangles at 275 K, green squares at 250 K, black pentagrams at 225 K and magenta diamonds at 200 K.

The ratio of the imaginary part of the permittivity to the real part gives the dielectric loss tangent, $\tan\delta$. Figure 4.7 shows that the conductivity of water dominates over dielectric storage above the freezing temperature, as $\tan\delta$ is higher than 1. However, water shows roughly equal conductive and dielectric behaviour below the freezing temperature ($\tan\delta \simeq 1$). The graph clearly implies that water and ice have different dipolar relaxation processes. The maximum value of $\tan\delta$ increases in water when the temperature decreases but decreases in ice. This behaviour was also observed by Abril et al. [18]. This indicates that water becomes more resistive and ice becomes relatively more dielectric at lower temperatures.

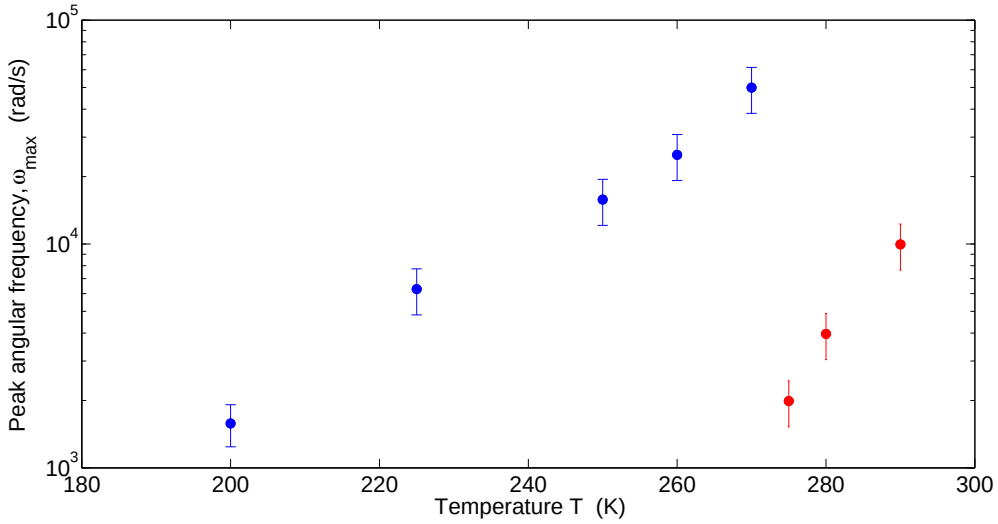

Figure 4.8: The angular frequency ω_{max} of the peak in $\tan\delta$ for water at different temperatures. The red circles represent water and the blue circles, ice.

Figure 4.8 shows the frequency ω_{max} of the peak in $\tan\delta$ as a function of T. ω_{max} increases with T in both ice and water. Since the characteristic relaxation time is inversely proportional to ω_{max}, this indicates that relaxation time decreases at high temperatures. A dramatic drop in ω_{max} can be seen when ice transforms into water while increasing temperature, indicating a transition between two relaxation processes.

We also performed experiments on water over the range of temperatures used in the PVA freeze-thaw cycles, using the same cooling and thawing rate. The real part of the permittivity was fitted using the Havriliak-Negami [18] equation explained in section 2.3.3. This equation described the data well for ice but not for water. Graphs of the data with the fitting function for ice are shown in Fig. 4.9. The fitting parameter values are presented in Table 4.1.

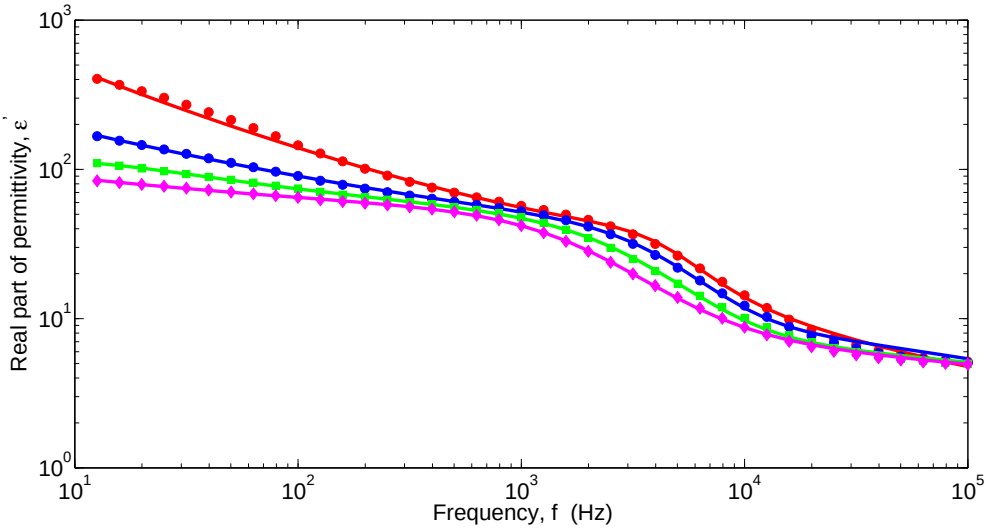

Figure 4.9: Real part of permittivity of ice at different temperatures. The solid lines show fits to the Havriliak-Negami equation at each temperature, with parameters given in Table 4.1. Red: 273 K, blue: 268 K, green: 263 K, and magenta: 253 K.

Table 4.1: Parameters from fits of the Havriliak-Negami equation to data for ice between 253 K and 273 K.

T (K)	$\Delta\varepsilon_{ep}$	τ_{ep} (s)	$\Delta\varepsilon_{\alpha}$	τ_{α} (μs)	σ_{dc} (mS/m)	β	γ	δ	ε_{∞}
253	220.29	1.87	42.91	76.0	1.69	0.32	1.2	0.88	2.81
258	226.02	0.97	43.35	56.7	-0.455	0.34	1.48	0.84	3.04
263	78.79	0.01	38.48	42.8	0.997	0.37	1.45	0.87	2.70
268	741.45	0.51	27.91	30.5	0.340	0.40	1.46	0.97	1.72
273	1385.66	0.07	19.14	34.6	0.851	0.54	0.81	1.29	2.04

The dielectric relaxation of water has been studied over different frequency ranges and temperatures previously [15, 18, 28]. The Debye equation has been successfully used to fit data for water above room temperature [15, 28] and the relaxation times have been found to be on the order of picoseconds. We were unable to adequately fit the data for water in Fig. 4.5, largely due to our low experimental frequencies which cannot capture the fast relaxation in liquid water. We were able to fit the data for ice as the relaxation time is longer in the solid phase. The trends in our fitting parameters are quite similar to those found in the work of Abril et al.[18] They found that the parameters β and δ did not vary appreciably with temperature.

The same is true for our data except at 273 K. The Debye relaxation time τ_α goes up when temperature decreases due to the decrease in the motion of the molecular dipoles.

4.2.2 Results for PVA cryogels

As mentioned above, PVA cryogels were tested in two ways: after completing a number of freeze-thaw cycles in the circulating bath, and while undergoing the cycles in the cryostat. First, we present data obtained by the former method. The dielectric constant of the samples was measured as a function of the frequency of the applied electric field at different temperatures. Figures 4.10 and 4.11 illustrate the real (dielectric constant) and imaginary (dielectric loss) parts of the permittivity of a PVA cryogel that had been subjected to one freeze-thaw cycle.

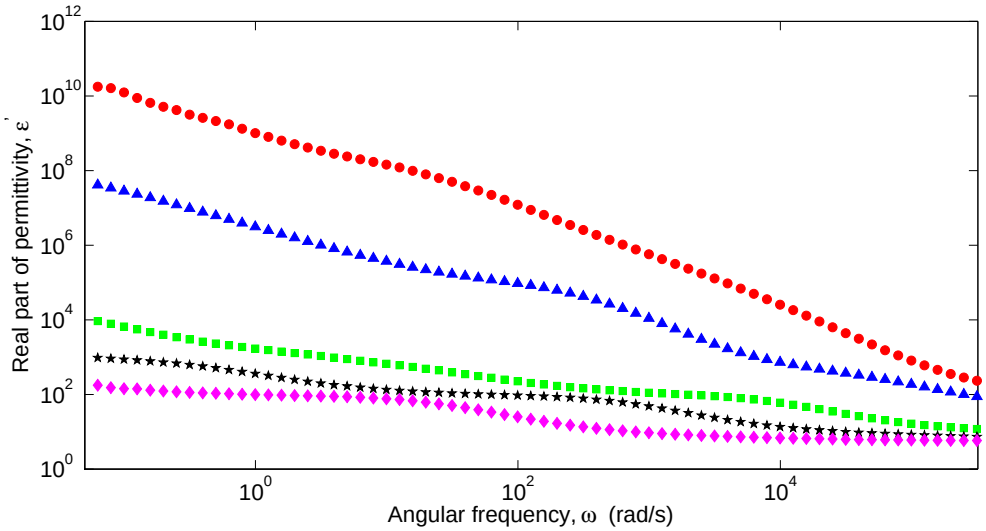

Figure 4.10: Real part of permittivity of a 1-cycle PVA cryogel at different temperatures: red circles at 290 K, blue triangles at 275 K, green squares at 250 K, black pentagrams at 225 K and the magenta diamonds at 200 K.

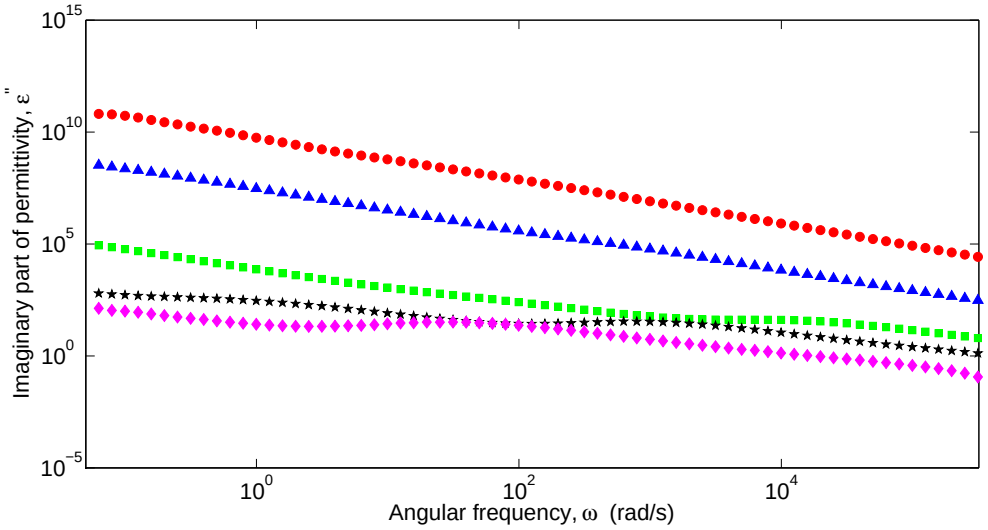

Figure 4.11: Imaginary part of permittivity of a 1-cycle PVA cryogel at different temperatures: red circles at 290 K, blue triangles at 275 K, green squares at 250 K, black pentagrams at 225 K and magenta diamonds at 200 K.

The increase in the real and imaginary parts of the permittivity at low frequencies is due to electrode effects of the capacitor, which are dominant at high temperatures. The plateau seen in the real part of the permittivity in Fig. 4.10 is due to dipole polarization. Though we expect the plateau at high frequencies, there is also a weak plateau at lower frequencies in the low temperature data, indicating the presence of two relaxation processes at different frequencies at low temperatures. There is no visible peak in the imaginary part of the permittivity at high temperatures, suggesting that the relaxation time is very short. In contrast, there is a weak peak in ε'' that shifts to lower frequencies at lower temperatures, indicating a slower relaxation process whose characteristic time scale increases as temperature decreases.

The three major features noticed in water can also be seen in Figs. 4.10 and 4.11. There are decreases in both parts of the permittivity with decreasing temperature and with increasing frequency, and a dramatic drop of the permittivity from 275 K to 250 K. Since the cryogel contains 88% water, the explanations for these features are the same as in water. The dielectric loss peak is not clearly visible due to the complexity of the material compared to the ideal

Debye material. In addition to these features, Fig. 4.10 shows more than one bump in ε' as a function of frequency. This is an indication of the presence of more than one relaxation process in this 1-cycle PVA cryogel. This can be seen more clearly by examining $\tan\delta$.

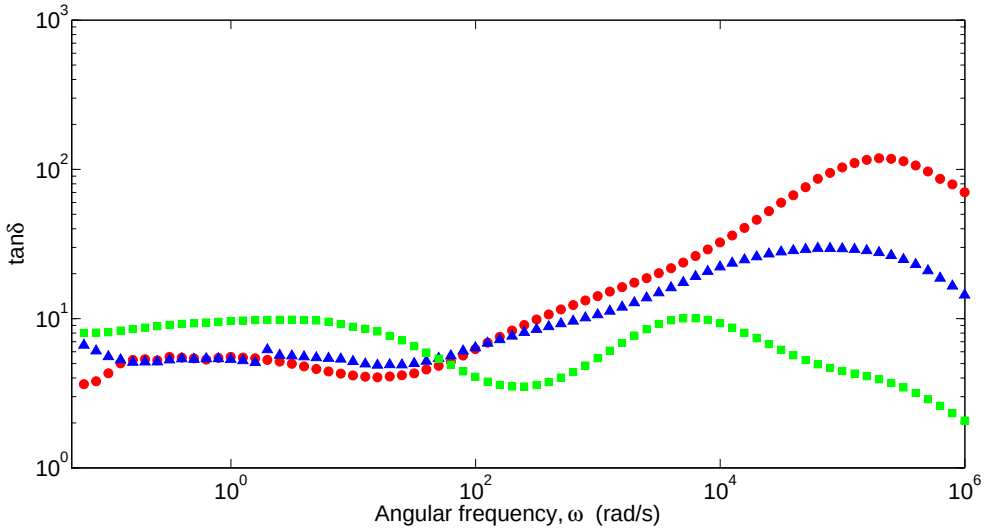

Figure 4.12: Dielectric loss tangent of a 1-cycle PVA cryogel at temperatures where liquid water is expected to be present: red circles at 290 K, blue triangles at 280 K and green squares at 275 K.

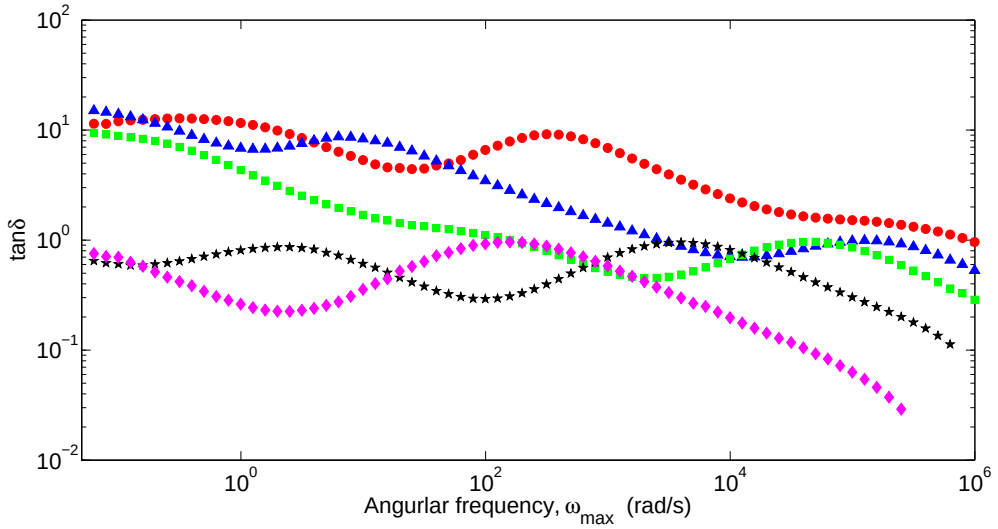

Figure 4.13: Dielectric loss tangent factor of 1-cycle PVA cryogel at temperatures below the freezing point of water: red circles at 270 K, blue triangles at 260 K, green squares at 250 K, black pentagrams at 225 K and magenta diamonds at 200 K.

Figures 4.12 and 4.13 present $\tan\delta$ versus frequency for a 1-cycle PVA cryogel at tem-

peratures where we expect the cryogel to contain liquid water (T≥273 K) and ice (T≤273 K) respectively. The appearance of several peaks in the graphs imply that there is more than one relaxation process in 1-cycle PVA cryogel.

The peak angular frequency ω_{max}, where the first derivative of $\tan\delta$ become zero, versus temperature is shown in Fig. 4.14. Based on the graph, we identify three possible relaxation processes in this 1-cycle PVA cryogel sample. All three possible relaxation processes are temperature dependant [13] and increase in frequency at high temperatures. The relaxation processes of PVA can be explained by the theory in Section 2.3.5. The process shown in red in Fig. 4.14 is identified with the β relaxation of PVA, i.e., relaxation of local dipoles as a result of small scale movements of parts of the PVA chains. The slower process shown in green in the graph is identified with α relaxation, which involves relaxation of the whole PVA chain. The third process is probably due to relaxation of water molecules, as discussed below.

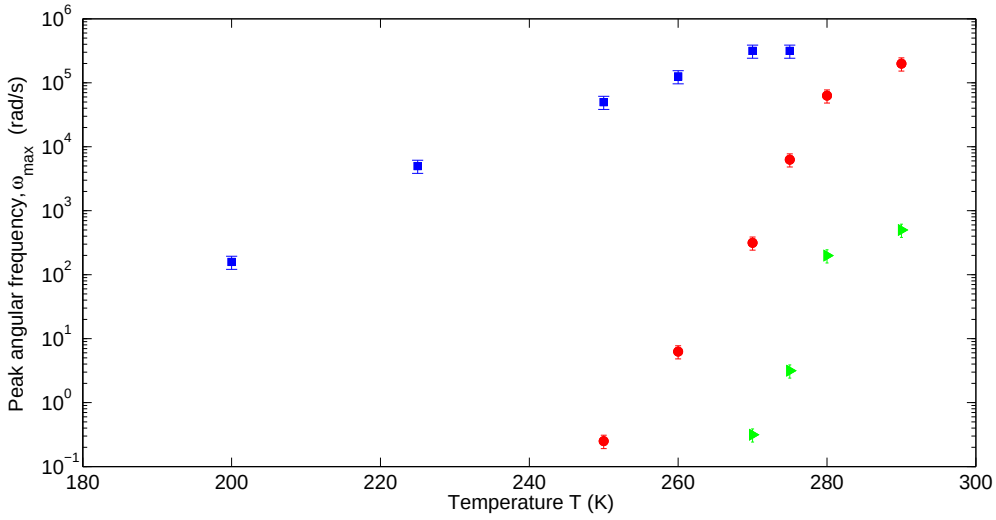

Figure 4.14: Angular frequency of the peaks in $\tan\delta$ for a 1-cycle PVA cryogel at different temperatures: The red circles are identified with β relaxation of PVA, the green triangles with α relaxation of PVA, and the blue squares with relaxation of water.

Figure 4.15 compares the peak frequencies corresponding to the three relaxation processes of the 1-cycle PVA cryogel to the frequencies measured for water and ice. We observe that

the frequencies of the third relaxation process of the 1-cycle PVA cryogel (blue squares in Fig. 4.15) are reasonably close to those for ice below 270 K.

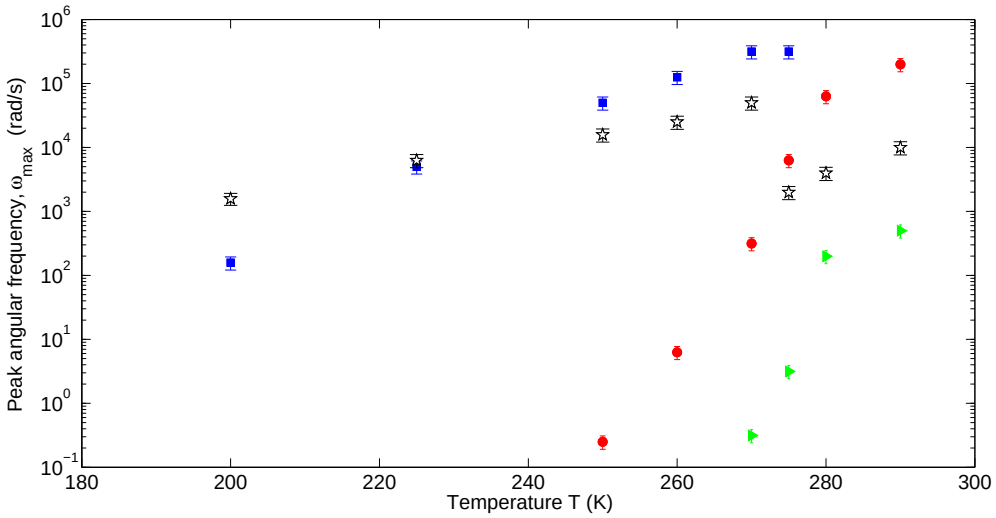

Figure 4.15: A comparison of peak angular frequency of a 1-cycle PVA cryogel (shown in Fig. 4.14) and water (shown in Fig. 4.8) at different temperatures. The symbols for the cryogel are the same as in Fig. 4.14. Data for water are shown as open black pentagrams.

Figure 4.16 illustrates the AC conductivity of a 1-cycle PVA cryogel versus frequency at different temperatures. Even pure water has a conductivity due to the presence of H^+, and OH^- ions. Ions in the water and charged impurities in the PVA provide the electrical charges that carry the current. The conductivity is higher at high temperatures, shows a dramatic drop from 275 K to 250 K and then continues the drop more slowly with decreasing temperature. After the first cycle, and at high temperatures, the PVA has a relatively small number of crosslinks. Therefore ionic transport is possible through the water and amorphous PVA regions. The drift velocity of the charges decreases when water transforms into ice, resulting in a decrease in conductivity of more than two orders of magnitude at all frequencies. The drop is close to four orders of magnitude at frequencies lower than 1 Hz. In addition, the conductivity decreases when the sample is cooled down due to a further reduction in the drifting of charges. The electrical conductivity of dried pure PVA was reported to be between 10^{-6} and 10^{-4} S/m at 298 K in the frequency range used in our experiments [29, 30]. Our measured conductivity is several

orders of magnitude higher, due to the presence of water in our samples. The frequency independent conductivity shown in Fig. 4.16 at higher temperatures implies that the 1-cycle PVA cryogel sample is more conductive than pure PVA. On the other hand it tends to behave more like an insulator at low temperatures. As discussed below, the charge transport mechanism changes for cryogels that have been subjected to more freeze-thaw cycles.

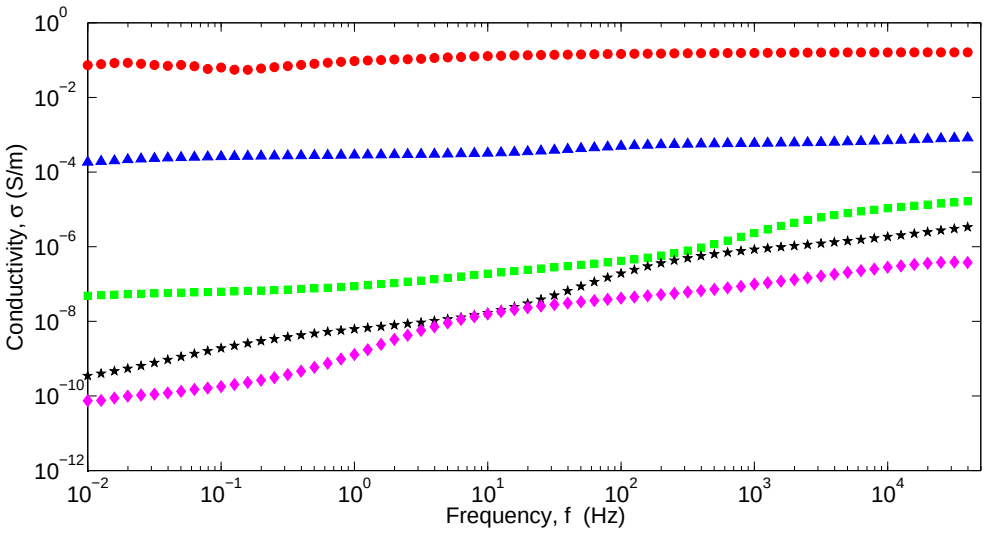

Figure 4.16: AC conductivity of a 1-cycle PVA at different temperatures: red circles: 290 K, blue triangles: 275 K, green squares: 250 K, black pentagrams: 225 K and magenta diamonds: 200 K.

The effect of the number of freeze-thaw cycles was also studied. All the samples discussed in this section completed their freeze-thaw cycles in the cooling bath before they were used for dielectric measurements.

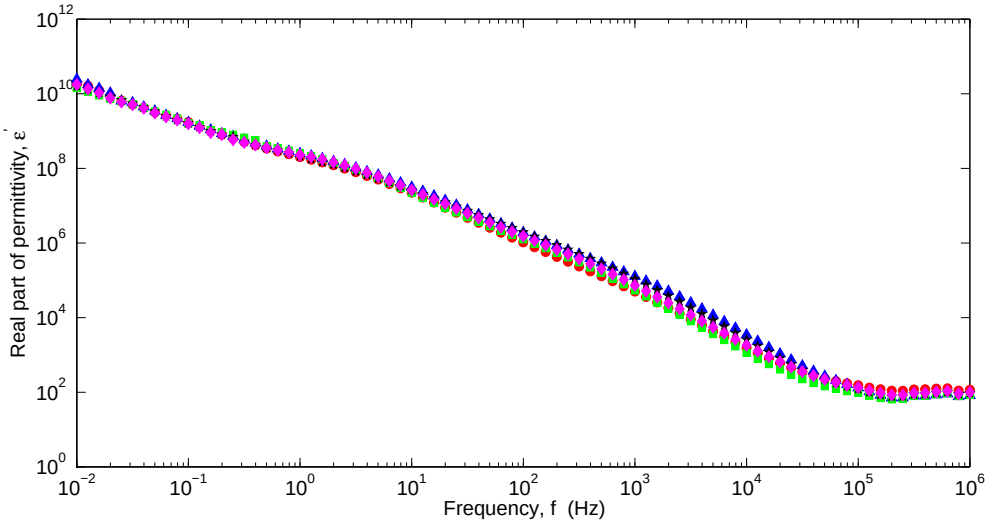

Figure 4.17: Real part of permittivity versus frequency for PVA cryogel samples made by changing the number of freeze-thaw cycles. The temperature was 290 K. Red circles: 1-cycle PVA cryogel, blue triangles: 2-cycle PVA cryogel, green squares: 3-cycle PVA cryogel, black pentagrams: 4-cycle PVA cryogel and magenta diamonds: 5-cycle PVA cryogel.

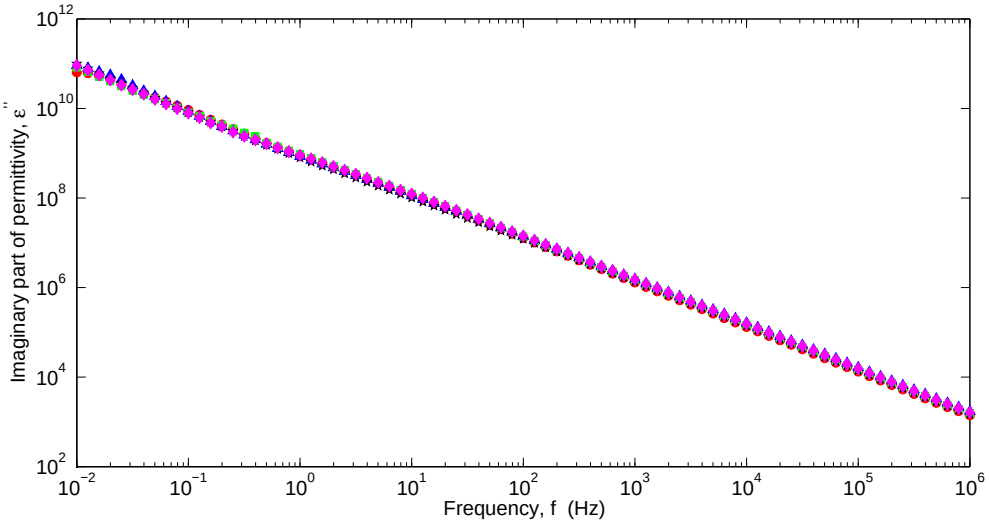

Figure 4.18: Imaginary part of permittivity versus frequency for PVA cryogel samples made by changing the number of freeze-thaw cycles. The temperature was 290 K. Red circles: 1-cycle PVA cryogel, blue triangles: 2-cycle PVA cryogel, green squares: 3-cycle PVA cryogel, black pentagrams: 4-cycle PVA cryogel and magenta diamonds: 5-cycle PVA cryogel.

The real and imaginary parts ε' and ε'' of the permittivity of the PVA cryogels are shown in Fig. 4.17 and Fig. 4.18, respectively. The continuous $1/f$ increase in ε' and ε'' implies that

the electrode effect is dominant over most of the frequency range studied at 290 K.

According to Figs. 4.17 and 4.18, the dielectric permittivity is almost independent of the number of freeze-thaw cycles. On the other hand, it is known that the number of crosslinks increases with the cycle number [31].

In a PVA solution, the polymer chains are relatively free to move. During the cooling stage of the first freeze-thaw cycle, the formation of ice concentrates the polymer in certain regions. Small PVA crystallites can form in these PVA-rich regions. The crystallites act as physical crosslinks between chains. In the heating portion of the cycle, the melting ice results in PVA poor regions surrounded by crosslinked PVA rich regions. Further freeze-thaw cycles form secondary crystallites in the amorphous PVA lying between the crosslinks made in the first cycle [31]. The crosslinking restricts dipole movement on the PVA chains even after one freeze-thaw cycle. Further restrictions that result from additional freeze-thaw cycles apparently do not cause a noticeable additional change in the permittivity. These results suggested that we should explore the changes in dielectric properties that take place during the freeze-thaw cycles to better understand the effects of physical crosslinking on the permittivity.

4.2.3 Cryogel in freeze-thaw cycles

Structural changes in PVA cryogels and their effects on dielectric properties can be investigated by taking measurements while the sample is undergoing a freeze-thaw cycle (steps shown in Fig. 4.19). For these experiments the experimental temperature range was restricted to between 293 K and 253 K as those were the boundary temperatures of each cycle. The cooling and thawing rates were maintained at $0.12\,\mathrm{K/min}$ for each cycle. The experimental frequency range was narrowed to 10^{-1} Hz $\leq f \leq 10^{6}$ Hz to reduce the time required to collect data so that each measurement is made at an approximately uniform temperature. In this Section, each sample was measured while it was undergoing a freeze-thaw cycle in the cryostat itself.

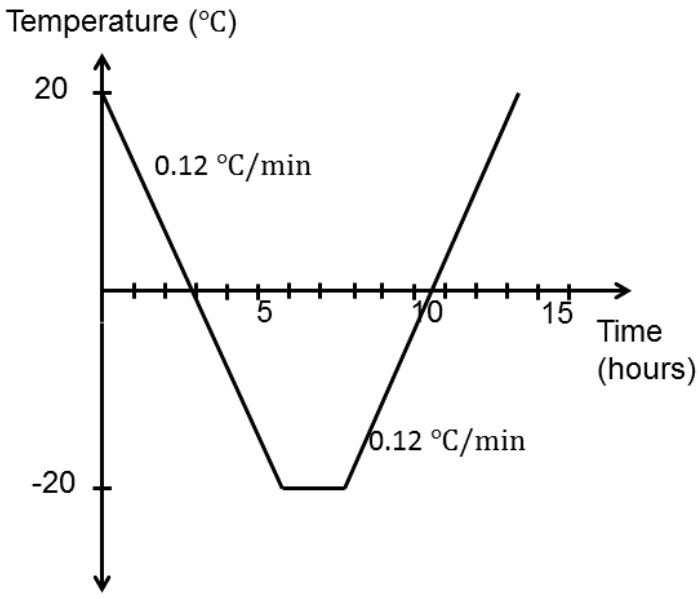

Figure 4.19: The three steps in a freeze-thaw cycle.The cooling and heating rate is 0.12 °C/min.

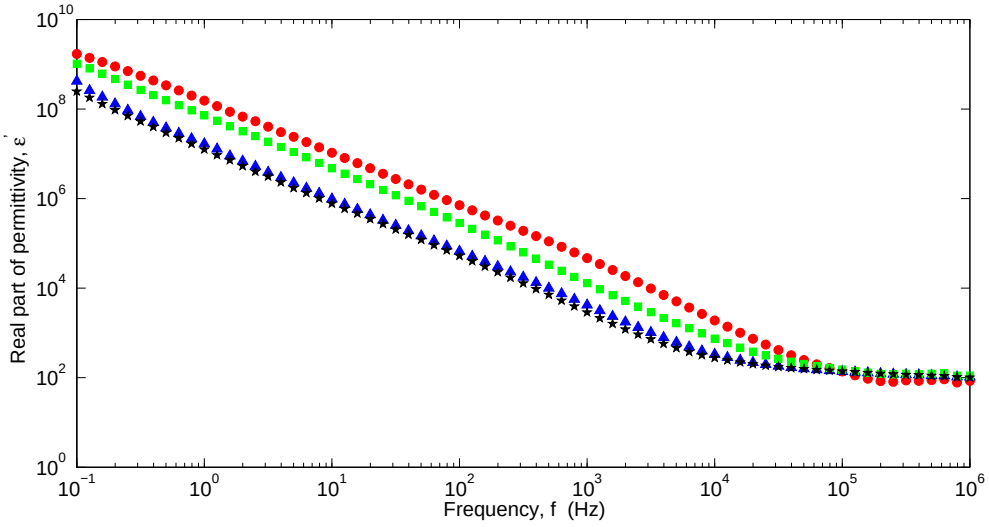

Figure 4.20: Real part of the permittivity of a PVA sample during the first freeze-thaw cycle at different temperatures: red circles at 293 K while the sample is cooling, green squares at 278 K while the sample is cooling, black pentagrams at 278 K while the sample is heating, blue triangles at 293 K while the sample is heating.

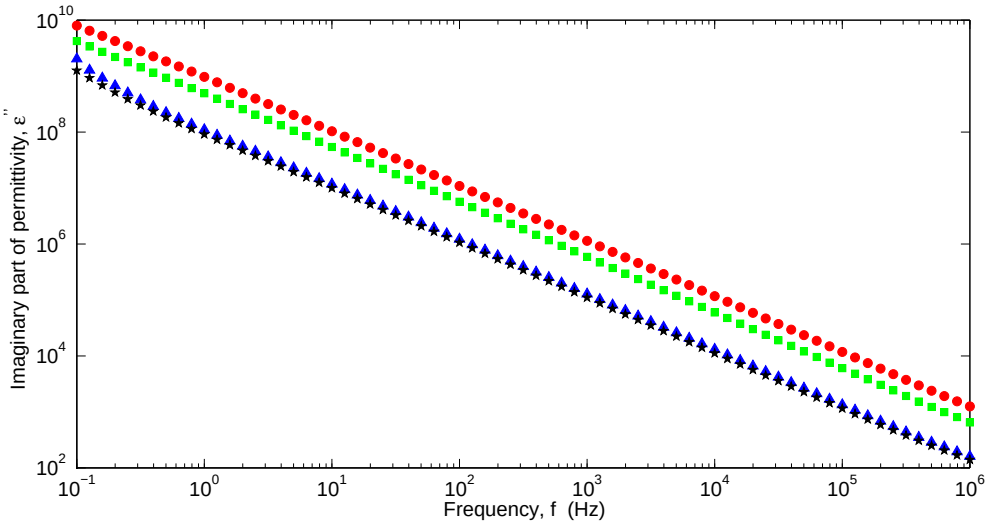

Figure 4.21: Imaginary part of the permittivity of a PVA sample during the first freeze-thaw cycle at different temperatures: red circles at 293 K while the sample is cooling, green squares at 278 K while the sample is cooling, black pentagrams at 278 K while the sample is heating, blue triangles at 293 K while the sample is heating.

The real and imaginary parts ε' and ε'' of the permittivity of a PVA cryogel are shown in Figs. 4.20 and 4.21, respectively. The high frequency plateau in the real part of the permittivity corresponds to dipole polarization, and the $1/f$ relationship of the imaginary part with frequency is mainly due to electrode polarization.

Figures 4.20 and 4.21 show that neither the real nor imaginary part of the permittivity return to their initial values after a cycle of cooling and heating. This implies that the physical microstructure of the PVA has changed due to physical crosslinking even after one freeze-thaw cycle, and also that this crosslinking affects the permittivity. At the beginning of the first cycle, the PVA sample was a solution. The PVA chains formed crosslinks due to partial crystalization while it was cooling down. When it is warmed back up from 253 K, only a fraction of the physical crosslinks disappear. The remaining crosslinks restrict the freedom of movement of dipoles on the polymer chains, leading to lower values of the permittivity.

As it is clear that the dielectric permittivity is affected by physical crosslinking, we studied

the changes in the permittivity that occurred as a PVA cryogel goes through different freeze-thaw cycles.

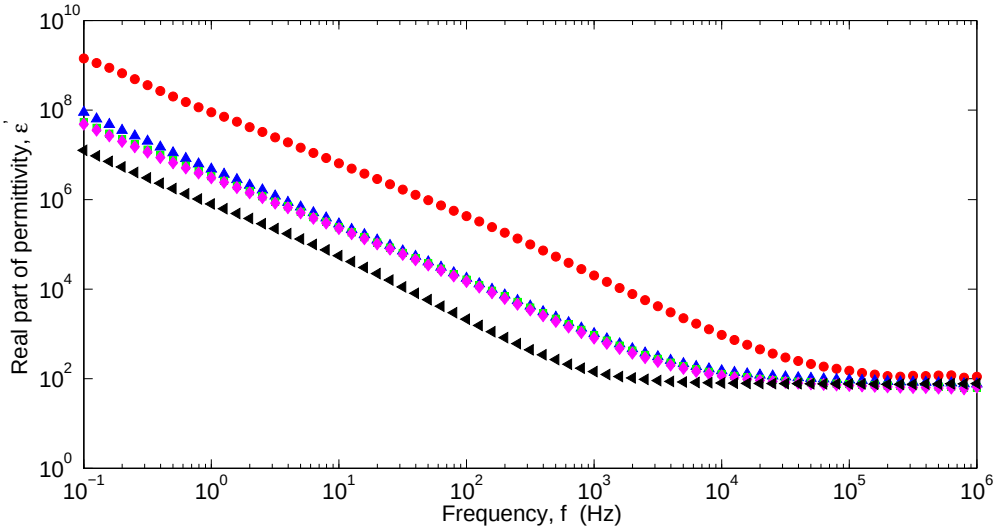

Figure 4.22: Real part of the permittivity of a PVA cryogel in different freeze-thaw cycles at 283 K. The data were taken while the sample is cooling down in each cycle: the red circles: in cycle 1, the blue triangles: in cycle 3, the green squares: in cycle 5, the magenta diamonds: in cycle 7. The black triangles are for water.

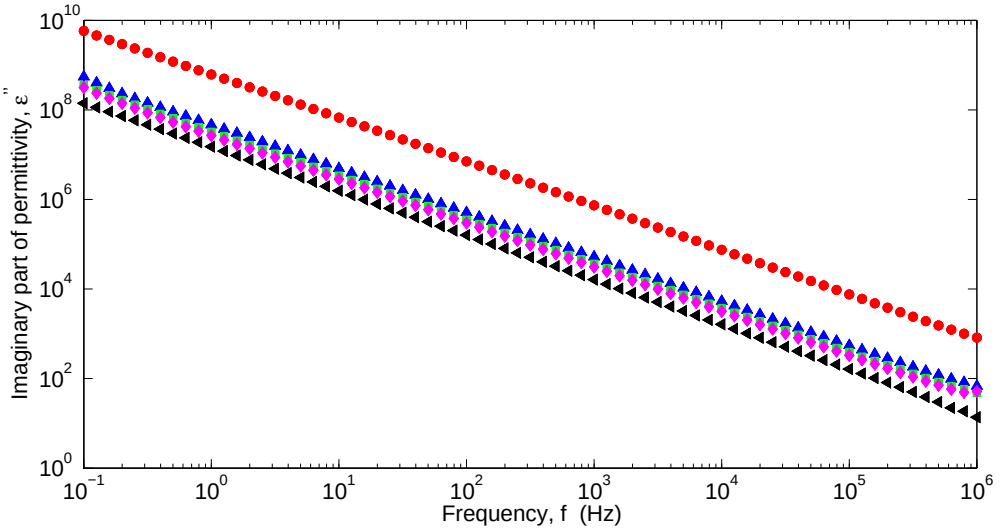

Figure 4.23: Imaginary part of the permittivity of a PVA cryogel in different freeze-thaw cycles at 283 K. The data were taken while the sample is cooling down in each cycle: the red circles: in cycle 1, the blue triangles: in cycle 3, the green squares: in cycle 5, the magenta diamonds: in cycle 7. The black triangles are for water.

ε' and ε'' for a PVA cryogel in different freeze-thaw cycles are shown in Figs. 4.22 and 4.23 respectively. As before, the imaginary part of the permittivity reflects the dominant electrode effect at lower frequencies, similar to Fig. 4.21.

Figures 4.22 and 4.23 indicate that the permittivity is nearly independent of the number of freeze-thaw cycles after the first cycle has been completed. This is consistent with what was shown in Figs. 4.17 and 4.18. Both real and imaginary parts reach values close to those for water after one complete cycle. This leads to the conclusion that the crosslinking of the polymer chains reduces the contribution of the PVA to the polarization, leading to low values for the permittivity. ε' is still a factor of ten larger for the cryogel than for water. At low frequencies, however, so the contribution of the PVA remains important. However at high frequencies ε' for the cryogel is very close to the value for water, indicating that the contribution of PVA chains is small at for $f \geq 10^4$ Hz. ε'' also shows some contribution due to PVA even after one cycle has been completed.

Figure 4.24 shows ε' for a PVA cryogel as a function of temperature as it goes through several freeze-thaw cycles at 1 kHz. Data for water are also shown. The transition temperature from water to ice can be found by studying the real part of the permittivity of water. The real part increases slowly below 273 K and more quickly above 273 K (shown in magenta). As expected, the transition happens at 273 K. For the PVA cryogel, a similar change in slope is seen at 273 K when the sample is in the cooling phase of the first cycle. The same data show a sudden drop of the real part of the permittivity at 263 K. This can be explained by the onset of PVA crystallization. The crystallization of the PVA restricts dipole movements in the PVA chains, decreasing the permittivity. Similar behaviour is observed at temperatures between 258 K and 263 K in later cycles. This indicates that there is a critical temperature around 263 K for the formation of PVA microcrystals in the PVA cryogel. In the heating portion of first and third cycles, ε' increases significantly around 268 K due to the PVA crystallites melting. This

shows that the crystallite melting temperature is higher than the crystallite freezing temperature. However, ε' is lower at the end of the cycle than at the beginning, indicating that some microcrystallization persists after the cycle. Previous works have used different minimum temperatures for their freeze-thaw cycles, but no critical temperature for microcrystallization of the PVA has been reported.

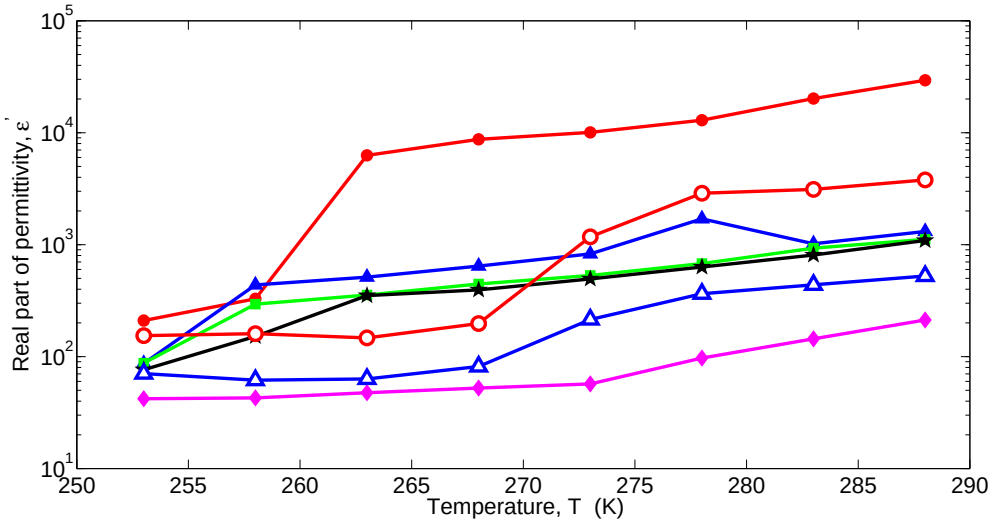

Figure 4.24: Real part of permittivity of a PVA cryogel as a function of temperature at 1 kHz. The data were taken while the sample in the freeze-thaw cycles. The lines are guide to the eye to follow water-ice transition temperature. The red solid circles for 1-cycle PVA cryogel cooling, the red open circles for 1-cycle PVA cryogel heating, the blue solid triangles for 3-cycle PVA cryogel cooling, the blue open triangles for 3-cycle PVA cryogel heating, the green squares for 5-cycle PVA cryogel cooling, the black pentagrams for 7-cycle PVA cryogel cooling. The magenta diamonds for water.

The dielectric relaxation processes of the PVA cryogels during different freeze-thaw cycles were studied by determining the frequency of the peaks ω_{max} in $\tan\delta$ as a function of frequency. Figure 4.25 shows the variation of ω_{max} for the β relaxation process of a PVA cryogel with the number of freeze-thaw cycles at 293 K. The data were taken while the PVA sample was at 293 K in the cooling portion of each cycle, that is, at the beginning of each cycle. The angular frequency of the peak is independent of the number of cycles after the first cycle has been completed. This implies that the time scale of the dielectric relaxation process does not change after the first cycle.

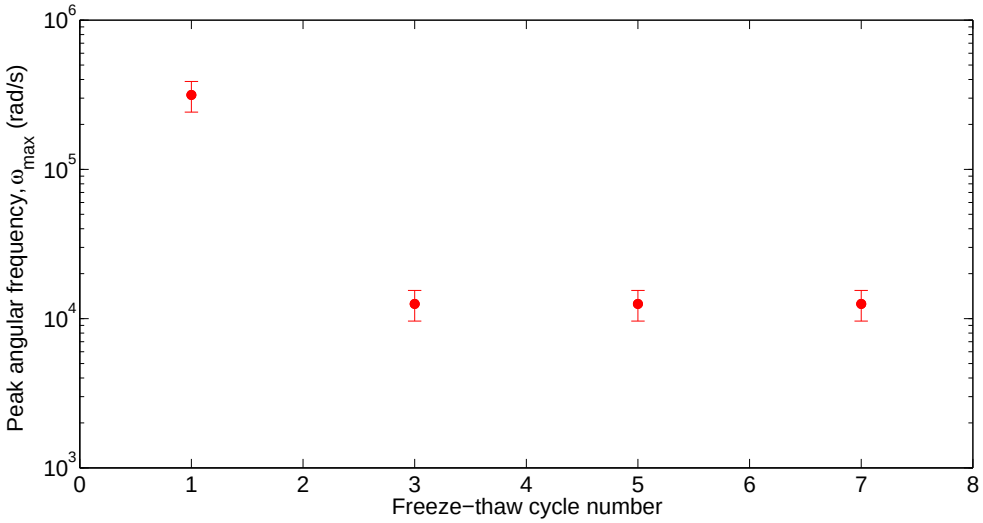

Figure 4.25: The peak angular frequency ω_{max} versus number of freeze-thaw cycles of a PVA cryogel at 293 K, at the beginning of each cycle.

The effect of the number of cycles on the AC conductivity can be seen in Fig. 4.26, which shows a decrease in σ with increasing number of freeze-thaw cycles. The conductivity of PVA during the first cycle is due to ionic transport in water and amorphous regions as explained in the previous section. Water and amorphous PVA can be present in the PVA crystallites as they are not perfect. Growth of the PVA crystallites during subsequent freeze-thaw cycles will reduce the amount of water and amorphous PVA in the crystallites. This would decrease the ion transport through the crystallites as the number and size of microcrystals increases. Charge transport in the crystalline regions would mainly be due to electron tunnelling and/or hopping. Electron trapping would be inevitable at the surface of the crystals and trapped charges could be ejected into the surrounding amorphous region, contributing to the electric current. The decrease in trapping and ion conduction through water in the crystalline regions result in lower current after more freeze-thaw cycles, as shown in Fig. 4.26.

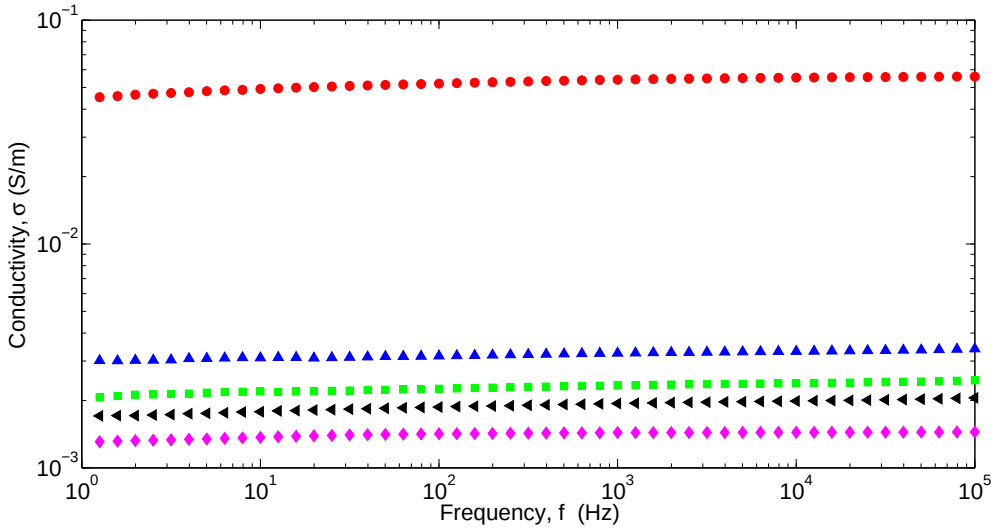

Figure 4.26: AC conductivity of a PVA cryogel and water at 288 K. PVA data were taken while cooling in each cycle: the red circles are for 1-cycle PVA cryogel, the blue triangles for 3-cycle PVA cryogel, the green squares for 5-cycle PVA cryogel, the black pentagrams for 7-cycle PVA cryogel and the magenta diamonds for water.

4.2.4 PVA nanocomposites

Since the results presented in the previous section show that the structure and dielectric properties of the PVA cryogels changed during the freeze-thaw cycles, PVA-CNT nanocomposites were also studied while undergoing thermal cycles in the cryostat. Data were recorded in the first, third and fifth freeze-thaw cycles.

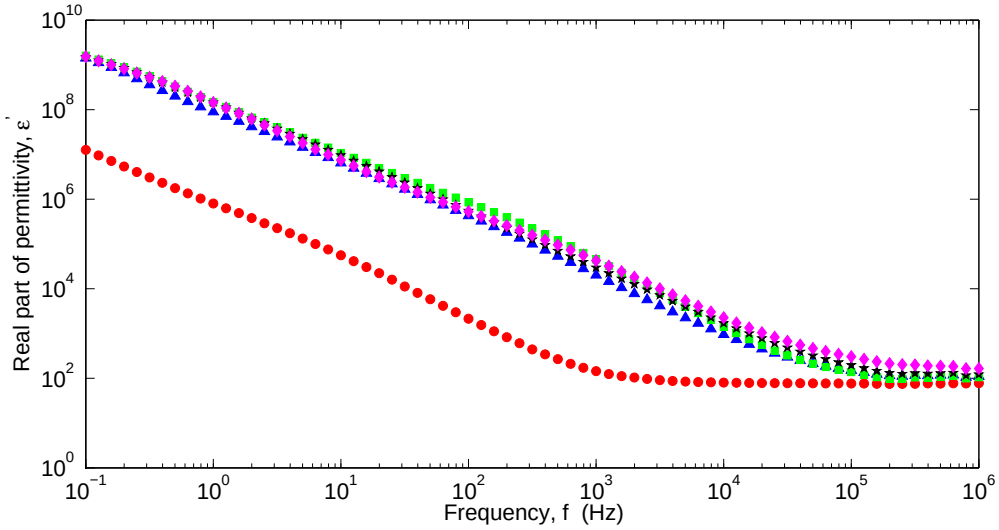

Figure 4.27: Real part of the permittivity of PVA nanocomposites at 283 K. The data were taken in the cooling portion of the first freeze-thaw cycle. The green squares are data for 0.1 wt% CNTs+PVA cryogel, the black pentagrams for 0.5 wt% CNTs+PVA cryogel and the magenta diamonds for 1.0 wt% CNTs+PVA cryogel. The blue triangles show data for PVA cryogel and the red circles for water under the same conditions.

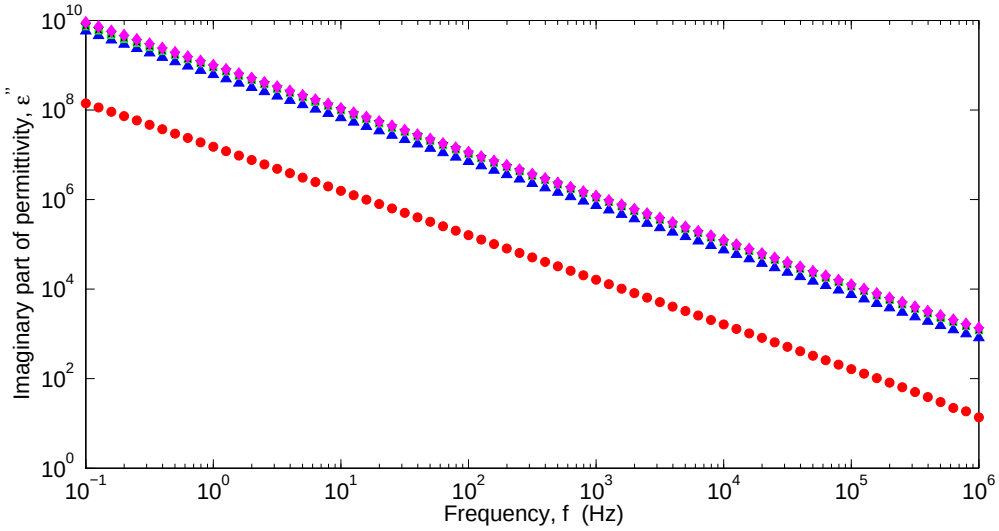

Figure 4.28: Imaginary part of the permittivity of PVA nanocomposites at 283 K. The data were taken in the cooling portion of the first freeze-thaw cycle. The green squares are data for 0.1 wt% CNTs+PVA cryogel, the black pentagrams for 0.5 wt% CNTs+PVA cryogel and the magenta diamonds for 1.0 wt% CNTs+PVA cryogel. The blue triangles show data for PVA cryogel and the red circles for water under the same conditions.

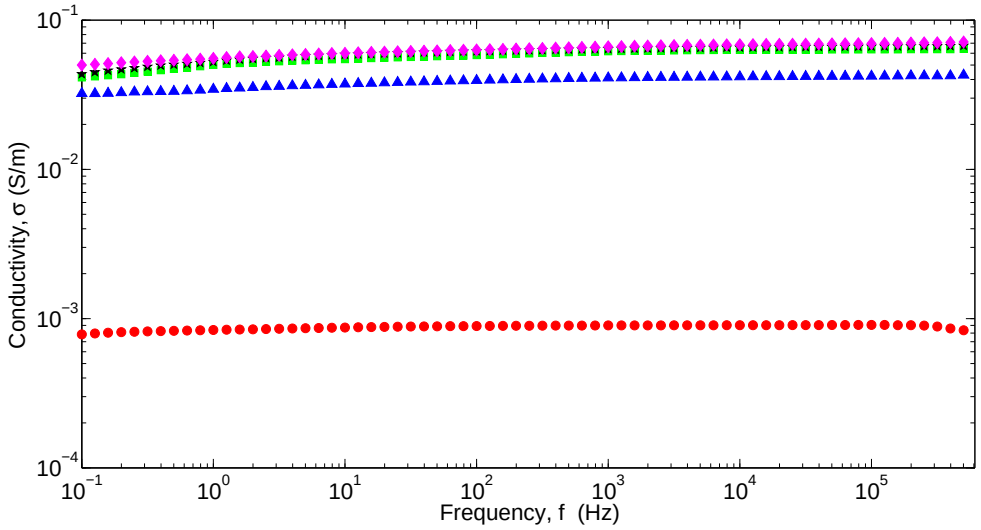

Figure 4.29: Conductivity of PVA nanocomposites at 283 K.The data were taken in the cooling portion of the first freeze-thaw cycle. The green squares are data for 0.1% CNT, the black pentagrams for 0.5% CNT and the magenta diamonds for 1% CNT. The blue triangles show data for PVA cryogel and the red circles for water under the same conditions.

The real and imaginary parts of the permittivity ε' and ε'' of PVA nanocomposites in the first freeze-thaw cycle are shown in Figs. 4.27 and 4.28 respectively. Similar to what was observed for the PVA cryogels, the electrode effect is dominant at lower frequencies, irrespective of the concentration of the nanotubes.

Figures 4.27 and 4.28 show that adding CNTs to PVA does not have much impact on either component of the permittivity. The real part of the permittivity changes slightly but not systematically. The imaginary part of the permittivity is higher than for the PVA cryogel, but is independent of the CNT concentration. As shown in Fig. 4.29, the conductivity of the PVA cryogel is higher than that of water, and adding CNT increases the conductivity further. The conductivity does not appear to depend strongly on the CNT concentration, however.

The small effect of the CNTs on the conductivity could be due to the higher conductivity of the PVA cryogels compared to pure PVA and saturation of conductive paths in the nanocomposite even for small CNT concentration. It was reported in previous work that CNT concentration

influenced the conductivity of dried polymer nanocomposites [5, 32], although samples studied in that work contained a polymer and CNTs but no water. For example, Juan et al.[32] measured the dielectric properties and conductivity of nanocomposites made by adding multi-walled carbon nanotubes to PVA and found that the percolation threshold was 0.675 wt%. If the CNTs are highly conductive, there should be a large increase in conductivity at percolation. However, we do not observe this increase. This could imply the CNTs have a low conductivity. It could also indicate that the CNT concentrations studies are below the percolation threshold.

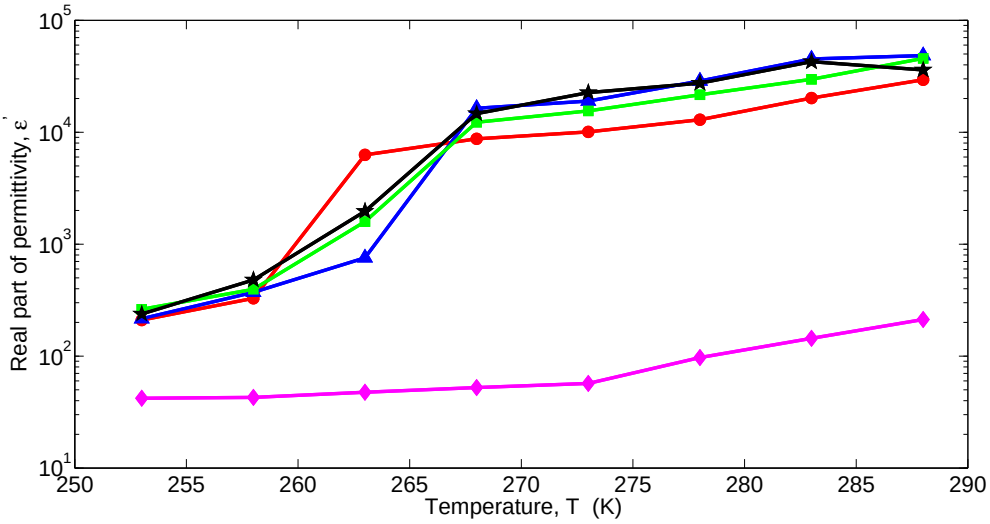

Figure 4.30: Real part of the permittivity of PVA nanocomposites versus temperature at 1 kHz. The data were taken in the cooling portion of the first freeze-thaw cycle. The blue triangles are data for PVA+0.1 % CNT, the green squares for PVA+0.5 % CNT, the black pentagrams for PVA+1 % CNT. The red circles show data for PVA cryogel and the magenta diamonds for water under the same conditions.

We found that ε' for PVA cryogels decreased significantly when they were cooled below 263 K as shown in Fig. 4.24. Figure 4.30 shows the same graph for PVA and the PVA-CNT nanocomposites in the first thermal cycle. Data for water are also shown for comparison. Comparing the two graphs it is noticeable that the temperature where ε' starts to decrease in the first cycle is shifted upwards to 268 K for the nanocomposites compared to 263 K for the pure PVA. Since we interpret the decrease in ε' to be due to the formation of the physical crosslinks via the formation of micro-crystals of PVA, this leads us to conclude that such crystallization is

enhanced by CNTs.

Figure 4.31 shows the variation of the real part of the permittivity of PVA-1% CNT nanocomposites with temperature over several thermal cycles. The permittivity decreases with temperature as shown in the previous figure. The temperature where ε' starts to decrease strongly decreases with increasing number of freeze-thaw cycles. The value of ε' at high temperatures decreases with the number of freeze-thaw cycles in contrast to what was observed in the PVA cryogel data shown in Fig. 4.24. This is further evidence for the enhancement of crystallization by CNTs.

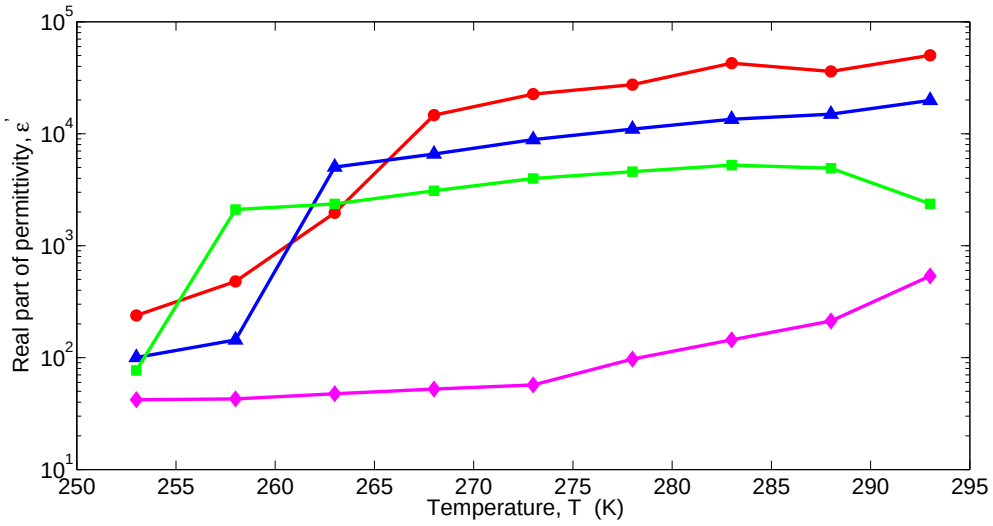

Figure 4.31: Real part of permittivity of PVA nanocomposites with 1% CNTs versus temperature at 1 kHz. The data were taken in the cooling portion of each cycle. The red circles are data for the nanocomposite in the first cycle, the blue triangles for the nanocomposite in the third cycle, the green squares for the nanocomposite in the fifth cycle, the black pentagrams for water under the same conditions.

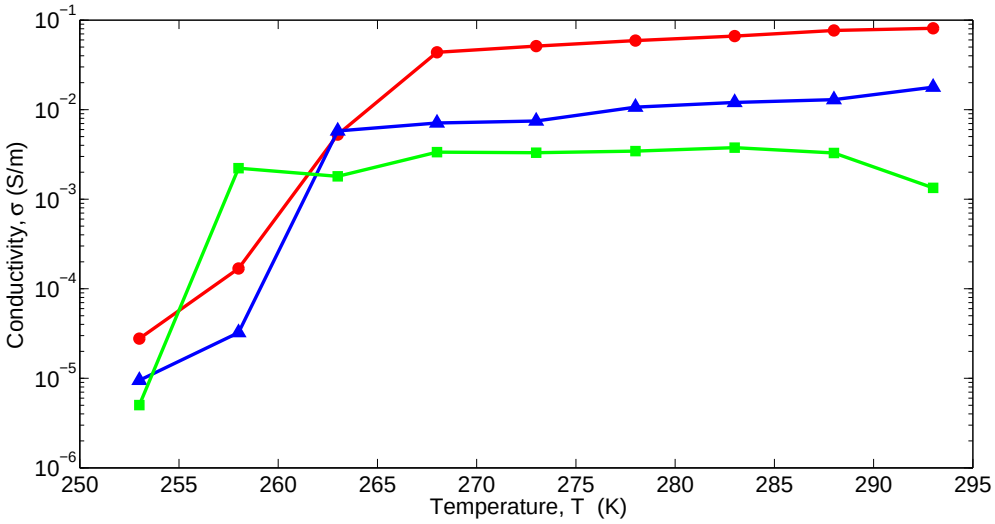

Figure 4.32: Conductivity of PVA nanocomposites with 1% CNTs versus temperature at 1 kHz. The data were taken while the samples are cooling down. The red circles for the nanocomposite in the first cycle, the blue triangles for the nanocomposite in the third cycle, the green squares for the nanocomposite in the fifth cycle.

We observed that conductivity of the PVA cryogel decreases with the number of freeze-thaw cycles, as shown in Fig. 4.26. We see the same behaviour in the PVA-CNT nanocomposites, as illustrated in Fig. 4.32. The conductivity also shows a sudden drop when $T < 268\,K$, which can also be interpreted as due to enhanced crystallization of the nanocomposite. The improved crystallization reduces the charge transport though the the sample, resulting in lower conductivity. It could also be due to a restriction of charge transport through CNTs resulting from interaction between the PVA chains and the CNTs.

Chapter 5

Discussion and Conclusions

In this work, we have used a dielectric spectrometer to study the complex permittivity and conductivity of polyvinyl alcohol (PVA) cryogels and nanocomposites made by adding single-walled carbon nanotubes (SWCNT) to PVA solutions. PVA solutions were made by dissolving the polymer in water, then PVA cryogels were made by subjecting the sample to a number of freeze-thaw cycles. As each sample contained more than 87% water, we first studied the dielectric spectrum of water. We then explored the complex permittivity and conductivity of PVA cryogels that had completed freeze-thaw cycles in the circulating bath and while they were undergoing the freeze-thaw cycles in the cryostat.

We observed three major features in the permittivity spectrum of water. Both real and imaginary parts of the permittivity decrease when the temperature goes down and decrease when frequency increases. Both ε' and ε'' drop dramatically in the temperature range of 275 K to 250 K as the water freezes. This is due to reduction of the movement of water dipoles in ice compared to water. We have observed that the frequency of the peak in $\tan\delta$ increases with increasing temperature implying that the relaxation time decreases as temperature increases [33, 34].

The dielectric response of PVA cryogels that were made in the circulating bath showed the same major features as did water. However, PVA cryogels show three relaxation process in $\tan\delta$. One process is attributed to relaxation of molecular dipoles in water. Another is identified with the β relaxation process, which involves the relaxation of local dipoles in the cryogel. The lowest frequency relaxation process is identified with the α process, which involves relaxation of the entire PVA chains. We directly observed that the cryogels became physically stronger with the number of cycles. This is due to continuous increase in the amount of microcrystallization. The original crystallites made in the first cycle grow in size, and secondary crystallites form with further cycles [31] which increases the mechanical strength of the cryogel [9]. Surprisingly, however, we found that the permittivity was independent of the number of freeze-thaw cycles. Water and hydroxyl groups on the PVA chain are the main contributors to the permittivity. After the first freeze-thaw cycle, the motion of dipoles on the of PVA chains is restricted by crystallization. Any further restriction that results from secondary crystallization is apparently too small to affect the permittivity spectrum.

The real and imaginary parts of the permittivity of PVA samples that were thermally cycled in the cryostat changed over the course of the first freeze-thaw cycle. It was observed that both parts of the permittivity were lower in the heating portion than in the cooling portion of the first cycle at 293 K and 278 K. This decrease is due to crystallization that occurs during the cooling process. However, there were no noticeable changes in the permittivity after the first freeze-thaw cycle. This leads us to conclude that the most of the structural changes that affect the permittivity of the cryogels happen in the first thermal cycle. These structural changes are caused by the primary crystallization that takes place during the cooling process. Previous studies [10, 32] have explored the electrical properties of PVA and its nanocomposites subjected to freeze-thaw cycles. To our knowledge, there have been no previous studies of cryogels while they undergo each freeze-thaw cycle.

We observed a critical temperature at which significant changes in the dielectric constant begin. The critical temperature for PVA cryogel was approximately 263 K for the first cycle and varied between 263 K and 258 K for subsequent cycles. Previous studies [7, 8, 9, 31] have not reported a particular critical temperature at which most physical changes occurred. When the temperature of the PVA solution decreases, the crystallization of PVA continues slowly. However the biggest change occurs at the critical temperature. The formation of PVA micro-crystals restricts motion of OH groups resulting in a drop in the permittivity at this temperature. During the heating phase of the thermal cycle, some bit of all of the crystallites melt, resulting in a partial recovery of ε'.

The complex permittivity and conductivity of PVA nanocomposites were studied to understand the effect of CNTs on electrical properties of PVA. All the nanocomposite data were measured while the samples were undergoing freeze-thaw cycles in the cryostat. The nanocomposites also showed a critical temperature at which the permittivity began to change significantly. However, the critical temperature for the nanocomposites was higher than for the cryogels, being about 268 K in the first freeze-thaw cycle. The critical temperature decreases for subsequent cycles. Adding SWCNTs increases the conductivity of the cryogel, but the increase is independent of the CNT concentration over the range we studied. The conductivity of the PVA-CNT nanocomposites decreases as the material goes through more freeze-thaw cycles. Interactions between the PVA chains and CNTs may reduce charge transport through the CNTs.

In this work, we have studied the dielectric properties of water, PVA solution, PVA cryogel and PVA nanocomposites. Overall, we have shown that dielectric spectroscopy can provide useful information about materials based on polymer solutions. One main results of this study is that we have provided a better physical picture of what happens to PVA solutions when they undergo freeze-thaw cycles. Starting from a solution, the PVA transforms into the gel state as a result of the crystallization of small regions of polymer. We have shown the existence of a

critical temperature for this microcrystallization at approximately 263 K. Our dielectric data have shown that most of the changes in the permittivity of cryogels happen during the first thermal cycle, although the mechanical properties of the cryogels continue to change in later cycles. This is not well understood and would be an interesting topic for further study. Adding CNTs to the PVA solution raises the critical temperature, and the resulting nanocomposites show continued changes in ε' in later cycles. Future work could investigate the interactions between CNT and PVA molecules in an attempt to explain this.

Though some precautions have been taken by the instrument to overcome electrode polarization, it is still very noticeable in our data at lower frequencies. Many previous studies have addressed the electrode effect and relaxation times by fitting their data to variety of models [12, 14, 16, 17]. However most of our data for PVA and its nanocomposites was not well described by any of those equations. This is presumably due to the complexity of our materials. It would be useful in future work to develop a model that can better explain the dielectric properties of PVA and its nanocomposites. It would also be interesting to carry out experiments over a larger range of CNT concentrations to look for a percolation threshold. This work could also be extended to study the dielectric properties of polymer nanocomposites based on other polymers, made with CNTs or other conductive particles.

Bibliography

[1] M.L. Hallensleben. Polyvinyl compounds, others. *Ullmann's Encyclopedia of Industrial Chemistry*, 2000.

[2] R.D.K. Misra, P. Nerikar, K. Bertrand, and D. Murphy. Some aspects of surface deformation and fracture of 5–20% calcium carbonate-reinforced polyethylene composites. *Materials Science and Engineering: A*, 384:284–298, 2004.

[3] A.T. DiBenedetto. Tailoring of interfaces in glass fiber reinforced polymer composites: a review. *Materials Science and Engineering: A*, 302:74–82, 2001.

[4] M. Rubinstein and R.H. Colby. *Polymer Physics*. Oxford University Press, 2003.

[5] P. Pötschke, S.M. Dudkin, and I. Alig. Dielectric spectroscopy on melt processed polycarbonate/multiwalled carbon nanotube composites. *Polymer*, 44:5023–5030, 2003.

[6] C.M. Hassan and N.A. Peppas. Structure and applications of poly (vinyl alcohol) hydrogels produced by conventional crosslinking or by freezing/thawing methods. In *Biopolymers· PVA Hydrogels, Anionic Polymerisation Nanocomposites*, pages 37–65. Springer, 2000.

[7] B.J. Ficek and N.A. Peppas. Novel preparation of poly (vinyl alcohol) microparticles without crosslinking agent for controlled drug delivery. In *Materials Research Society Symposium Proceedings*, volume 331, pages 223–226. Materials Research Society, 1994.

[8] K. Tamura, O. Ike, S. Hitomi, J. Isobe, Y. Shimizu, and M. Nambu. A new hydrogel and its medical application. *American Society of Artificial Internal Organs Journal*, 32:605–608, 1986.

[9] L.E. Millon, M.-P. Nieh, J. L. Hutter, and W. Wan. SANS characterization of an anisotropic poly (vinyl alcohol) hydrogel with vascular applications. *Macromolecules*, 40:3655–3662, 2007.

[10] M.E. Londoño, J.M. Jaramillo, R. Sabater, and J.M. Vélez. Dielectric properties of poly (vinyl alcohol) hydrogels prepared by freezing/thawing technique. *Revista EIA*, 18:105–114, 2012.

[11] K.J.M. Surry, H.J.B. Austin, A. Fenster, and T.M. Peters. Poly(vinyl alcohol) cryogel phantoms for use in ultrasound and MR imaging. *Physics in Medicine and Biology*, 49:5529–5546, 2004.

[12] A.R. Blythe and D. Bloor. *Electrical Properties of Polymers*. Cambridge University Press, 2005.

[13] J.P. Runt and J.J. Fitzgerald. *Dielectric Spectroscopy of Polymeric Materials*. American Chemical Society, 1997.

[14] A. Chelkowski. *Dielectric physics*. Polish Scientific, 1980.

[15] R. Buchner, J. Barthel, and J. Stauber. The dielectric relaxation of water between 0 °C and 35 °C. *Chemical Physics Letters*, 306:57–63, 1999.

[16] K.S. Cole and R.H. Cole. Dispersion and absorption in dielectrics I. alternating current characteristics. *The Journal of Chemical Physics*, 9:341–351, 1941.

[17] S. Havriliak and S. Negami. A complex plane representation of dielectric and mechanical relaxation processes in some polymers. *Polymer*, 8:161–210, 1967.

[18] A. Angulo-Sherman and H. Mercado-Uribe. Water under inner pressure: A dielectric spectroscopy study. *Physical Review E*, 89:022406, 2014.

[19] S.O. Kasap. *Principles of Electronic Materials and Devices, Third Edition*. McGraw-Hill, 2006.

[20] http://www.solartronanalytical.com/index.aspx, (last accessed on August 03, 2015).

[21] *Materials Test System User Guide*. Solartron Analytical Ltd., 2011.

[22] http://www.lakeshore.com/products/cryogenic-temperature-controllers/model-335/pages/overview.aspx, (last accessed on August 03, 2015).

[23] J.Y. Chang, D.Y. Godovsky, M.J. Han, C.M. Hassan, J. Kim, B. Lee, Y. Lee, N.A. Peppas, R.P. Quirk, and T. Yoo. *Biopolymers, PVA Hydrogels, Anionic Polymerisation, Nanocomposites*. Springer, 2000.

[24] N. Kazemi-Zanjani, P. Gobbo, Z. Zhu, M.S. Workentin, and F. Lagugné-Labarthet. High-resolution Raman imaging of bundles of single-walled carbon nanotubes by tip-enhanced Raman spectroscopy. *Canadian Journal of Chemistry*, 93:51–59, 2014.

[25] K. Flavin, I. Kopf, E. Del Canto, C. Navio, C. Bittencourt, and S. Giordani. Controlled carboxylic acid introduction: a route to highly purified oxidised single-walled carbon nanotubes. *Journal of Materials Chemistry*, 21:17881–17887, 2011.

[26] L.E. Millon, H. Mohammadi, and W.K. Wan. Anisotropic polyvinyl alcohol hydrogel for cardiovascular applications. *Journal of Biomedical Materials Research Part B: Applied Biomaterials*, 79:305–311, 2006.

[27] P. Ehrlich. Dielectric properties of teflon from room temperature to 314 °C and from frequencies of 102 to 105 c/s. *Journal of Research of the National Bureau of Standards*, 51:185–188, 1953.

[28] U. Kaatze. Complex permittivity of water as a function of frequency and temperature. *Journal of Chemical and Engineering Data*, 34:371–374, 1989.

[29] A. Fattoum and M. Arous. Conductivity and dielectric relaxation in various polyvinyl alcohol/ammonium salt composites. *Polymer Science Series A*, 56:907–916, 2014.

[30] H.N. Chandrakala, B. Ramaraj, and G.M. Madhu. The influence of zinc oxide–cerium oxide nanoparticles on the structural characteristics and electrical properties of polyvinyl alcohol films. *Journal of Materials Science*, 47:8076–8084, 2012.

[31] P.J. Willcox, D.W. Howie, K. Schmidt-Rohr, D.A. Hoagland, S.P. Gido, S. Pudjijanto, L.W. Kleiner, and S. Venkatraman. Microstructure of poly (vinyl alcohol) hydrogels produced by freeze/thaw cycling. *Journal of Polymer Science Part B: Polymer Physics*, 37:3438–3454, 1999.

[32] J. Zhang, M. Mine, D. Zhu, and M. Matsuo. Electrical and dielectric behaviors and their origins in the three-dimensional polyvinyl alcohol/mwcnt composites with low percolation threshold. *Carbon*, 47:1311–1320, 2009.

[33] A. Von Hippel. The dielectric relaxation spectra of water, ice, and aqueous solutions, and their interpretation 1. *Critical survey of the status-quo for water. IEEE Trans. Electr. Insul*, 23:801–816, 1988.

[34] *Dielectric relaxation of ice samples grown from vapor-phase or liquid-phase water*, Berlin, Germany, 2009. Springer.

Curriculum Vitae

Name:	Nuwansiri Getangama
Post-Secondary Education and Degrees:	University of Sri Jayewardenepura 2006–2010 B.Sc. Nugegoda, Sri Lanka
Honours and Awards:	Western Graduate Research Scholarship 2013–2015 Western Graduate Teaching and Research Assistanship 2013–2015
Related Work Experience:	Teaching Assistant Department of Physics and Astronomy The University of Western Ontario 2013–2015 Teaching Assistant Department of Physics University of Sri Jayewardenepura 2010–2012
Conferences	Poster presentation at Canadian Association of Physicist (CAP) conference, University of Alberta, Edmonton, AB, June 15, 2015-June 19,2015. Dielectric Spectroscopy of Polyvinyl Alcohol Hydrogels and Nanocomposites.